2013

Plasma Membrane Compartmentalization of D2 Dopamine Receptors

Meenakshi Sharma
University of Rhode Island

Jeremy Celver
University of Rhode Island

See next page for additional authors

Citation/Publisher Attribution
Sharma, M., Celver, J., Octeau, J. C., & Kovoor, A. (2013). Plasma Membrane Compartmentalization of D2 Dopamine Receptors. *Journal of Biological Chemistry, 288*, 12554-12568. doi: 10.1074/jbc.M112.443945
Available at: http://dx.doi.org/10.1074/jbc.M112.443945

THE JOURNAL OF BIOLOGICAL CHEMISTRY VOL. 288, NO. 18, pp. 12554–12568, May 3, 2013

Plasma Membrane Compartmentalization of D2 Dopamine Receptors*

Received for publication, December 10, 2012, and in revised form, February 26, 2013 Published, JBC Papers in Press, March 14, 2013, DOI 10.1074/jbc.M112.443945

Meenakshi Sharma, Jeremy Celver[1], J. Christopher Octeau, and Abraham Kovoor[2]

From the Department of Biomedical and Pharmaceutical Sciences, University of Rhode Island, Kingston, Rhode Island 02881

Background: Plasma membrane microcompartmentalization could provide multiple unique environments for the operation of different signaling pathways.
Results: An in-cell biotin transfer assay showed highly restricted cellular accessibility for a detergent-resistant but functional pool of plasma membrane-expressed D2 dopamine receptor (D2R).
Conclusion: D2R is segregated in special plasma membrane microcompartments.
Significance: Our data provide one of the first definitive demonstrations of plasma membrane microcompartmentalization in living cells.

Plasma membrane microcompartments could allow different signaling pathways to operate more efficiently and prevent cross-talk. We utilized a novel in-cell biotin transfer assay to demonstrate that the majority of plasma membrane-expressed D2 dopamine receptor (D2R) is microcompartmentalized within detergent-resistant structures. Conversely, a minority of D2R existed in a detergent-soluble form and interacted in a relatively unrestricted manner with other cellular proteins. The microcompartmentalization of D2R had functional consequences because dopamine-induced internalization of D2R was largely restricted to the compartmentalized receptor. The D2R-containing microcompartments did not correspond to putative detergent-resistant lipid raft structures. First, the detergent-insoluble D2R structures were significantly denser than detergent-resistant membrane fragments containing flotillin, a widely utilized lipid raft marker protein. Second, the detergent solubility of D2R was unaffected by treatment of cells with the cholesterol chelating agent, methyl-β-cyclodextrin, that is thought to disrupt lipid rafts. Finally, the in-cell biotinylation assay did not provide any evidence for the membrane compartmentalization of peptide motifs thought to target to lipid rafts. Thus, our observations form one of the first demonstrations, in living cells, of plasma membrane microcompartments defined by the ability of the compartment structure to broadly restrict the interaction of resident molecules with other cellular proteins.

According to the fluid mosaic model, biological membranes can be considered as a two-dimensional fluid along which lipids and associated proteins are free to diffuse and interact with each other (1). However, the specificity of many membrane-associated biochemical reactions and the ability of cells to distinguish between the numerous signals transmitted across the membrane have led to suggestions that many proteins are microcompartmentalized in the membrane, although they appear to be uniformly distributed when examined using microscopic techniques (2, 3). Nevertheless, 4 decades after the proposal of the fluid mosaic model by Singer and Nicolson (1), definitive proof of such plasma membrane microcompartments that exist in living cells to restrict non-resident components from interacting with resident molecules has not been presented.

Studies of model membranes indicated that rafts of cholesterol and certain lipid molecules (*e.g.* sphingolipids) could create less fluid areas within lipid membranes. Subsequently, buoyant detergent-resistant aggregations enriched in cholesterol, sphingolipids, and distinctive proteins were isolated after detergent solubilization of cellular material. These findings gave rise to the idea that such aggregations originated from lipid raft complexes that existed in living cells and functioned as membrane compartments that could include certain proteins and exclude others (4–6). However, no definitive evidence has been provided to show that detergent-resistant biochemical fractions necessarily originate from microdomains that existed in intact cells before detergent was added or for the existence of canonically defined lipid rafts in living cells (7–12). Detergent treatment alters the properties of both lipids and proteins, and it has been shown that aggregation or segregation of membrane components can occur as an artifact of detergent treatment (13, 14).

Evidence exists for small transient clusters of cholesterol, sphingolipids, and membrane proteins (3, 7, 11) and for the transient restriction of some proteins to submicroscopic regions of the plasma membrane (15). However, clustering and compartmentalization are distinct phenomena, and the biological relevance of these processes has been questioned because their half-lives are shorter than that of most protein-protein interactions (11).

* This work was supported, in whole or in part, by National Institutes of Health, NIMH, Grant R15MH091639 (to A. K. and M. S.) and a Rhode Island Institutional Development Award (IDeA) Network of Biomedical Research Excellence (INBRE) Award, P20RR016457–10, from the National Center for Research Resources (NCRR), National Institutes of Health.
[1] To whom correspondence may be addressed: University of Rhode Island, 7 Green House Rd., Kingston, RI 02881. Tel.: 401-874-4727; E-mail: jeremy.celver@hotmail.com.
[2] To whom correspondence may be addressed: University of Rhode Island, 7 Green House Rd., Kingston, RI 02881. Tel.: 401-874-4727; E-mail: abekovoor@uri.edu.

The D2 dopamine receptor (D2R)[3] is a clinically important G protein-coupled receptor because it is a major target of drugs used to alleviate symptoms of Parkinson disease and depression (16, 17). In addition, a common property of all currently available antipsychotic drugs is that they block D2R at therapeutic concentrations (18).

We previously showed that the vast majority of D2R expressed in the brain is uniquely resistant to detergent solubilization (19) and wanted to explore the biological significance of our observation. We utilized a novel in-cell biotin transfer assay involving the *Escherichia coli* biotin ligase enzyme, BirA, that specifically attaches biotin to a unique acceptor peptide (AP) (20). We 1) attached AP to D2R, 2) fused the biotin ligase enzyme to a wide variety of cellular proteins, and 3) in a series of experiments, introduced the D2R-AP target and a biotin ligase enzyme-fusion into living cells. After the cells were solubilized in detergent we found that, in almost every case, the biotinylation of the detergent-resistant form of D2R-AP substrate was barely detectable. Instead, most of the biotin was found attached to the detergent-soluble D2R-AP, which formed less than 25% of the total cellular D2R-AP. However, we showed that the detergent-resistant forms of both D2R and the D2R-AP fusion were functional and could respond to dopamine. The results from the above experiments provide the first clear demonstration, in living cells, of two functional populations of a plasma membrane protein that differ broadly in their level of compartmentalization from other cellular proteins.

MATERIALS AND METHODS

Chemicals—All chemicals and reagents were purchased from Sigma-Aldrich or Thermo Fisher Scientific or from suppliers specifically identified below.

Cell Culture—HEK293T cells (American Type Culture Collection, Manassas, VA) were maintained and transfected in Dulbecco's modified Eagle's medium (DMEM) with 10% fetal bovine serum (Sigma) supplemented with penicillin and streptomycin. The cells were grown at 37 °C and 5% CO_2. Transfection of cells was carried out using Lipofectamine LTX (Invitrogen) according to the manufacturer's instructions. Total transfected DNA was kept constant between groups using pcDNA3.1/Zeo(+) (Invitrogen) mammalian expression vector.

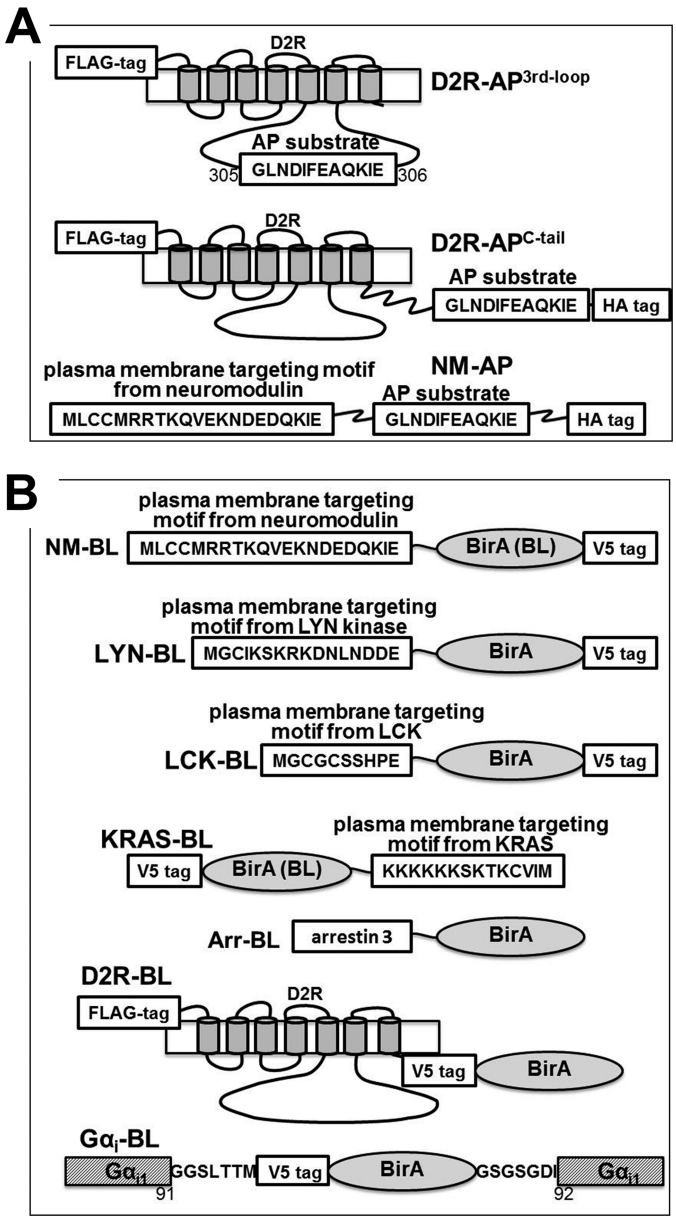

FIGURE 1. **Schematic representation (N- to C-terminal) of the complementary fusion proteins containing the AP substrate for BirA (*A*) and the BirA enzyme (*B*) that were utilized in this study.** *A*, the *numbers 305* and *306* in the *top panel* refer to the position of the residues in the third cytoplasmic loop of D2R between which the AP substrate was inserted. The *squiggly line* connecting the AP substrate to D2R in the *center panel* represents a flexible 106-amino acid linker from the constant region of the human immunoglobulin κ_1-light-chain constant region. *B*, in the *bottom panel*, the *numbers* represent the amino acid residues in the $G\alpha_{i1}$ between which the V5 tag and the BirA enzyme were inserted.

cDNA Constructs—The cDNAs for the constructs described below were assembled using standard molecular biology protocols. All of the constructs, except for the neuromodulin/GAP-43 (NM)-AP fusion substrate, were cloned into the mammalian expression vector pcDNA3.1/Zeo(+) (Invitrogen). The cDNA for NM-AP was inserted into the pJ602 mammalian expression vector (DNA 2.0). Schematics of the various protein constructs used in this study are shown in Fig. 1.

The cDNA for the FLAG-tagged D2R and μ-opioid receptor (MOR) constructs have been previously described and consist

[3] The abbreviations used are: D2R, D2 dopamine receptor long isoform; Arr, arrestin3; AP, acceptor peptide substrate for the biotin ligase enzyme with amino acid sequence of GLNDIFEAQKIEWHE; BirA, *E. coli* biotin ligase; BL, biotin ligase enzyme; D2R-AP$^{3rd\text{-}loop}$, D2 dopamine receptor long isoform fused to the AP substrate for the BL enzyme to the third cytoplasmic loop; D2R-AP$^{C\text{-}tail}$, D2 dopamine receptor long isoform fused to the AP substrate tethered to the cytoplasmic C-tail of D2R; EZ-Link sulfo-NHS-LC-biotin, sulfosuccinimidyl 6-(biotinamido) hexanoate; FLAG, octapeptide with amino acid sequence of DYKDDDDK; HA tag, a peptide with amino acid sequence YPYDVPDYA from human influenza HA; HEK293T, human embryonic kidney 293 cells stably expressing the SV40 T-antigen; KRAS-BL, KRAS-derived plasma membrane-targeting motif-biotin ligase protein fusion construct; LCK-BL, LCK kinase-derived plasma-membrane targeting motif-biotin ligase protein fusion construct; LYN-BL, LYN kinase-derived plasma-membrane targeting motif-biotin ligase protein fusion construct; MβCD, methyl-β-cyclodextrin; MOR, μ-opioid receptor; NM, neuromodulin-derived plasma membrane-targeting motif; TX100, Triton X-100; V5 tag, a peptide with amino acid sequence of GKPIPNPLLGLDST; ANOVA, analysis of variance; RBE, relative biotinylation efficacy.

of the FLAG epitope tag attached to the extracellular N terminus of the human D2R (long form) and mouse MOR, respectively (21).

The cDNA for the fusions of D2R with an attenuated AP substrate sequence (GLNDIFEAQKIE) (20) for the *E. coli* biotin ligase, BirA, contained the FLAG epitope tag at the extracellular N terminus. D2R-AP$^{3rd\text{-}loop}$ fusion was constructed by inserting the AP sequence between positions 305 and 306 (amino acids Leu and Thr) in the third cytoplasmic loop of FLAG-tagged human D2R long form. The D2R-AP$^{C\text{-}tail}$ fusion was constructed by tethering AP to the cytoplasmic C-tail of the FLAG-tagged D2R construct via a flexible 106-amino acid linker corresponding to the constant region (amino acids 131–236; see GenBank^{TM} entry AAD29608.1) of the human immunoglobulin κ_1-light-chain constant region (IgκC). The D2R-AP$^{C\text{-}tail}$ also contained an HA epitope tag (YPYDVPDYA) at the C terminus. Thus, the D2R-AP$^{C\text{-}tail}$ construct consisted of the following fused peptide sequences, in order, from the N to the C terminus: FLAG epitope-tagged human D2R long form, IgκC, AP substrate sequence (GLNDIFEAQKIE), and HA epitope tag.

NM-AP consisted of the following fused peptide sequences, in order, from the N to the C terminus: the membrane-targeting peptide sequence (MLCCMRRTKQVEKNDEDQKI) from NM (22), a 7-amino acid (GSGGGSG) flexible linker, the AP substrate, and the GSGGGSG linker followed by the HA epitope tag.

The cDNA for the *E. coli* biotin ligase, BirA (20), was provided by Dr. Alice Ting (Massachusetts Institute of Technology) and was amplified by standard PCR for use in the construction of the BirA-containing fusions. The BirA fusions used to biotinylate the AP substrate-containing constructs were composed of the following sequences and were inserted in the pcDNA3.1/Zeo(+) vector. The neuromodulin-biotin ligase fusion, NM-BL, consisted of a membrane-targeting peptide sequence from NM, fused to the N terminus of the *E. coli* biotin ligase, BirA, via a 5-amino acid flexible linker (GSGSG). The fusion was labeled at the C terminus with the V5 epitope tag, GKPIPNPLLGLDST. Thus, the NM-BL fusion construct consisted of the following fused peptide sequences, in order, from the N to the C terminus: the NM membrane-targeting peptide, the GSGSG linker, BirA, and the V5 epitope tag. The LYN kinase-biotin ligase fusion (LYN-BL) consisted of the following fused peptide sequences, in order, from the N to the C terminus: a membrane-targeting peptide sequence (MGCIK-SKRKDNLNDDE) from LYN kinase, the GSGSG linker, BirA, and the V5 epitope tag. The LCK-biotin ligase fusion (LCK-BL) consisted of the following fused peptide sequences, in order, from the N to the C terminus: a membrane-targeting peptide sequence (MGCGCSSHPE) from the kinase, LCK, the GSGSG linker, BirA, and the V5 epitope tag. The KRAS-biotin ligase fusion (KRAS-BL) consisted of the following fused peptide sequences, in order from the N to the C terminus: the V5 epitope tag, BirA, the GSGSG linker, and a membrane-targeting peptide sequence (KKKKKKSKTKCVIM) from KRAS. Note that the membrane-targeting sequence from KRAS is present at the C terminus of the endogenous KRAS protein, and hence this membrane targeting sequence was attached to the very C terminus of the fusion protein.

The arrestin3-biotin ligase fusion (Arr-BL) consisted of the following fused peptide sequences, in order, from the N to the C terminus: bovine arrestin3 (GenBank^{TM} accession number NP_001192206), the GSGSG linker, and BirA. The D2R-biotin ligase fusion (D2R-BL) was constructed by tethering BirA, tagged at the N terminus with the V5 epitope tag, to the C-tail of the FLAG epitope-tagged D2R construct described above. The biotin ligase construct, BL, consisted of the *E. coli* biotin ligase, BirA, tagged at the C terminus with the V5 epitope.

The G protein-biotin ligase fusion ($G\alpha_i$-BL) was constructed by inserting BirA tagged at the N terminus with the V5 epitope between positions 91 and 92 (amino acids Leu and Lys, respectively) of the pertussis toxin-insensitive C351G mutant of human $G\alpha_{i1}$ (GenBank^{TM} accession number P63096). The V5-tagged BirA enzyme was inserted into an internal position within the primary sequence of $G\alpha_{i1}$ and not into the N or C terminus because the G protein $G\alpha$ N-terminal region is important for association with the G protein $G_{\beta\gamma}$ dimer, and the C-terminal region is required for interaction with receptors. Therefore, the V5 epitope-tagged BirA enzyme was inserted into a loop within α-helical domain of the $G\alpha_{i1}$ subunit. Insertion of various sequences into $G\alpha$ subunits at this position has been previously shown to allow the $G\alpha$ subunits to retain important functions, such as activation by receptors and the modulation of important effectors (23, 24). The PCR and cloning steps utilized in the construction of this fusion resulted in the introduction of the peptide sequences GGSLTTM and GSGSGDI, flanking the N and C terminus of the V5-BirA insertion, respectively. Thus, the $G\alpha_i$-BL fusion construct consisted of the following fused peptide sequences in order from the N to the C terminus: $G\alpha_{i1}$ fragment 1–91, the peptide sequence GGSLTTM, the V5 epitope tag, BirA, the peptide sequence GSGSGDI, and the $G\alpha_{i1}$ C351G mutant fragment 92–353.

Cell Surface Biotinylation—HEK293T cells were transiently transfected with cDNA for either the extracellular N-terminal FLAG-tagged D2Rs, the D2R-AP$^{C\text{-}tail}$ construct (tagged at the C terminus with the HA epitope tag), or the N-terminal FLAG-tagged MORs in a 6-well plate (4×10^5 cells/well) and cultured for 48 h to allow for transient expression of the respective protein constructs. Proteins expressed specifically at the surface of the cultured cells were biotinylated using EZ-Link Sulfo-NHS-LC-Biotin (Thermo Fisher Scientific, Pierce), a membrane-impermeable biotinylation reagent that reacts with primary amines of peptides projecting out into the extracellular space (25, 26). The cells were treated with the biotinylation reagent at a concentration of 1 mg/ml for 30 min at 4 °C according to the manufacturer's instructions. After the biotinylation reaction had occurred, the cells were washed three times in phosphate-buffered solution (PBS; 137 mM NaCl, 2.7 mM KCl, 10 Na_2HPO_4, 2 mM KH_2PO4, pH 7.4) containing glycine (100 mM) at 4 °C to remove and quench excess biotinylation reagent. The cells were then lysed in PBS (500 μl/well) containing 2% (v/v) of the non-ionic detergent, Triton X-100 (TX100), and a protease inhibitor mixture (SIGMAFAST^{TM} protease inhibitor mixture tablets with EDTA, Sigma-Aldrich) for 1 h at 4 °C. The cell lysates in each well were then separately centrifuged at $10,000 \times g$ for 10 min at 4 °C to sediment the TX100-insoluble (pellet) cellular fraction, and the TX100-insoluble pellet was

resuspended in 100 μl of 2% SDS-containing buffer (2% (w/v) SDS, 10 mM EDTA, 50 mM Tris-HCl, SIGMAFAST™ protease inhibitor mixture, pH 7.5). Both the TX100-soluble fraction (supernatant from the centrifugation) and the TX100-insoluble fraction that was resuspended in SDS buffer were incubated at 65 °C for 15 min. Subsequently, dilution buffer (6 mM EDTA, 2% (v/v) TX100, SIGMAFAST™ protease inhibitor mixture) was added to the TX100-insoluble fraction to reduce the SDS concentration to 0.2% (w/v). Dilution buffer was also added to the solution containing the TX100-soluble fraction (supernatant from centrifugation) so as to equalize the volume with the solution containing the TX100-insoluble cellular fraction, and both sets of solutions were cooled on ice. The biotinylated cell surface proteins were then extracted from the respective solutions using streptavidin-agarose resin (Thermo Fisher Scientific, Pierce). 50 μl of the resin, previously washed three times with wash buffer (150 mM NaCl, 6 mM EDTA, 50 mM Tris-HCl, 0.1% (v/v) TX100, pH 7.5), was added to each of the solutions and incubated at 4 °C with shaking for 1 h. The agarose resin was separated by centrifugation (8000 × *g* for 1 min) and then washed three times in wash buffer. The protein bound to each of the resin aliquots was eluted into 50 μl of SDS sample buffer (2% (w/v) SDS, 50 mM Tris-HCl, 50 mM DTT, 0.1% (w/v) bromphenol blue, pH 6.8) by incubating in a boiling water bath for 10 min. Equal volumes of the extracted protein-SDS sample buffer solutions were subjected to SDS-PAGE, and the resolved proteins were transferred to methanol-wetted polyvinylidene fluoride (PVDF) membranes by Western blotting. The relative amounts of the D2R and MOR constructs that segregated into the TX100-soluble and -insoluble plasma membrane fractions were determined as described under "Western Blotting and Quantification of Protein Signals." FLAG-tagged D2R and MOR were detected on the blots using the M2 anti-FLAG tag mouse monoclonal antibody (Sigma-Aldrich), and the HA epitope-tagged D2R-AP$^{C\text{-}tail}$ construct was detected using the HA.11 anti-HA tag mouse monoclonal antibody (Covance). The native D2R was detected using a polyclonal rabbit antibody (TH-50, Santa Cruz Biotechnology, Inc., Santa Cruz, CA).

Receptor Internalization Assay—HEK293T cells were transiently transfected with cDNA for either the extracellular N-terminal FLAG-tagged D2R or the HA epitope-tagged D2R-AP$^{C\text{-}tail}$. Approximately 48 h post-transfection, cells were treated with dopamine (10 μM from a stock of 10 mM dopamine that contained 5 mM ascorbic acid to inhibit dopamine oxidation) for 30 min and then were washed three times with ice-cold PBS to stop further receptor trafficking. The amount of D2R remaining at the cell surface was estimated relative to control D2R-expressing cells that were treated with vehicle, utilizing the protocol described under "Cell Surface Biotinylation." Briefly, the cell surface proteins were specifically biotinylated with membrane-impermeable EZ-Link Sulfo-NHS-LC-Biotin reagent and then lysed in TX100. The amounts of biotinylated D2R that segregated into either the TX100-soluble or -insoluble fractions of dopamine-treated cells was estimated relative to the corresponding D2R signal from cells that were treated only with vehicle. We confirmed that the total amount of biotinylated protein that could be detected in the TX100-soluble and insoluble fractions was not altered by dopamine treatment by probing Western blots of these samples with horseradish peroxidase (HRP)-conjugated streptavidin.

Estimation of the Relative Buoyancies of TX100-insoluble D2R-containing and Flotillin-containing Cellular Membrane in Sucrose Solutions—1×10^6 HEK293T cells were plated per well of a 6-well cell culture plate and transiently transfected with cDNA for the FLAG-tagged D2R construct. 48 h post-transfection, the cells from 2 wells of the plate were combined and lysed in TNE lysis buffer (25 mM Tris-HCl, 150 mM NaCl, 5 mM EDTA, SIGMAFAST protease inhibitor mixture, 2% (v/v) TX100, pH 7.5) for 1 h at 4 °C. The cell lysates were centrifuged at 10,000 × *g* for 10 min at 4 °C to pellet the TX100-insoluble fractions. The TX100-insoluble pellet was then resuspended by sonication with a probe sonicator (XL-2000, Qsonica LLC; three pulses of 0.5 s at power setting 4) in 700 μl of the TNE lysis buffer. 100-μl volumes of the resuspended TX100-insoluble cellular membranes were then layered onto separate solutions of TNE buffer (25 mM Tris-HCl, 150 mM NaCl, 5 mM EDTA, SIGMAFAST protease inhibitor mixture, pH 7.5) containing sucrose at concentrations (w/v) of 30, 40, 50, 60, 70, 80, and 90%, respectively, and centrifuged at 10,000 × *g* for 1 h at 4 °C. The proteins in the TX100-insoluble membranes that were pelleted in each tube were dissolved in 100 μl of SDS-urea sample buffer. The proteins in the TX100-insoluble membrane that remained buoyant in the supernatant were precipitated by the addition of trichloroacetic acid (TCA; final concentration of 10% (w/v)), washed three times with cold (4 °C) acetone and, air-dried and dissolved in 100 μl of SDS-urea sample buffer. Equal volumes of the protein-SDS-urea sample buffer solutions were resolved by SDS-PAGE, and the relative levels of transiently expressed D2R and endogenously expressed flotillin that either remained buoyant or sank to the bottom (pellet fraction) of each of the sucrose cushions were determined as described under "Western Blotting and Quantification of Protein Signals." FLAG-tagged D2R was detected on the blots using the M2 anti-FLAG tag mouse monoclonal antibody (Sigma-Aldrich). Flotillin was detected using anti-flotillin 1 rabbit polyclonal antibody (Sigma-Aldrich).

Methyl-β-cyclodextrin (MβCD) Treatment—HEK293T cells were transiently transfected with cDNA for the HA epitope-tagged D2R-AP$^{C\text{-}tail}$. 48 h post-transfection, the cell culture medium was replaced with serum-free DMEM, and the cells were treated in the serum-free DMEM with 10 mM sterile filtered MβCD (Acros Organics) for 1 h at 37 °C. The cell surface proteins were specifically biotinylated using the membrane-impermeable EZ-Link Sulfo-NHS-LC-Biotin reagent, and then the biotinylated TX100-soluble and -insoluble proteins were separated, isolated, resolved on SDS-PAGE, and Western blotted as described under "Cell Surface Biotinylation." The relative levels of transiently expressed D2R and endogenously expressed flotillin that segregated into the TX100-soluble and -insoluble plasma membrane fractions from cells treated with either MβCD or vehicle were determined as described under "Western Blotting and Quantification of Protein Signals." FLAG-tagged D2R was detected on the blots using the M2 anti-FLAG tag mouse monoclonal antibody (Sigma-Aldrich), and the HA epitope-tagged D2R-AP$^{C\text{-}tail}$ construct was detected using the HA.11 anti-HA tag mouse monoclonal antibody

(Covance). Flotillin was detected using anti-flotillin 1 rabbit polyclonal antibody (Sigma-Aldrich).

Biotinylation of D2R-AP and NM-AP Fusions in TX100-soluble and -insoluble Fractions by Fusions Containing the E. coli Biotin Ligase, BirA—HEK293T cells cultured in biotin-depleted media (2×10^5 cells/well of 12-well plates, plated 24 h before transfection) were transiently co-transfected with cDNAs for one of the AP substrate-containing fusions, D2R-AP$^{3rd\text{-}loop}$ or D2R-AP$^{C\text{-}tail}$ or NM-AP, and a complementary biotin ligase fusion. Biotin-free medium was prepared by incubating the complete medium (*i.e.* supplemented with fetal bovine serum, glutamine, and antibiotics) for 30 min at 20 °C with 30 μl/ml high capacity streptavidin-agarose resin (Thermo Fisher Scientific, Pierce; the agarose resin was pre-washed three times with PBS) and filtered using 2-μm pore size nylon syringe filters (Thermo Fisher Scientific). Approximately 48 h post-transfection, the cells were washed twice with PBS at 20 °C and then incubated for 5 min at 37 °C with PBS containing 10 μM biotin and washed again with cold (4 °C) PBS to remove biotin. In the next step, the cells were lysed in PBS (200 μl/well) containing 2% (v/v) TX100 and SIGMAFAST protease inhibitor mixture for 1 h at 4 °C. The cell lysates in each well were then separately centrifuged at 10,000 $\times$ *g* for 10 min at 4 °C to sediment the TX100-insoluble (pellet) cellular fraction, and the TX100-insoluble fraction was resuspended in 100 μl of 2% SDS-urea sample buffer (2% (w/v) SDS, 8 M urea, 50 mM Tris-HCl, 50 mM DTT, 0.1% (w/v) bromphenol blue, pH 6.8) for 15 min at 65 °C. The TX100-soluble proteins in the supernatant solution were precipitated by the addition of TCA (final concentration of 10% (w/v)), washed three times with cold (4 °C) acetone, air-dried, and dissolved by incubation for 15 min at 65 °C in 100 μl of SDS-urea sample buffer. Equal volumes of the protein-SDS-urea sample buffer solutions were resolved by SDS-PAGE and transferred to PVDF membrane by Western blotting. The relative levels of biotinylated AP substrate-containing fusions segregating into the TX100-soluble and -insoluble cellular fractions were estimated by probing the blots with streptavidin conjugated to HRP as described under "Western blotting and Quantification of Signals." AP substrate-containing fusion protein levels and the biotin ligase-containing fusion protein levels in each of the cellular fractions were estimated by probing duplicate blots with antibodies directed against the epitope tags, either FLAG, HA, or V5, that were engineered into the fusions.

Fluorescent Labeling and Confocal Laser-scanning Microscopy—We utilized fluorescent labeling methods in conjunction with confocal laser microscopy to visualize the subcellular distribution and localization of the D2R-AP$^{3rd\text{-}loop}$ substrate protein, the biotinylated D2R-AP$^{3rd\text{-}loop}$ substrate, and the co-expressed biotin ligase fusion that mediated the biotinylation. The relative subcellular localization of the D2R-AP$^{3rd\text{-}loop}$ protein substrate and the subset of the D2R-AP$^{3rd\text{-}loop}$ protein that was biotinylated was visualized in the same cells using double-labeling techniques. The subcellular localization of the biotin ligase fusion was visualized in a separate set of cells. HEK293T cells were plated on BD BioCoat poly-D-lysine-coated 12-mm diameter glass coverslips (BD Biosciences) in 24-well plates (2×10^5 cells/well) and cultured using the biotin-depleted medium described above. After ~24 h, they were transiently co-transfected with cDNA for D2R-AP$^{3rd\text{-}loop}$ substrate and a biotin ligase fusion. Approximately 48 h post-transfection, the cells were washed twice with PBS at 20 °C and then incubated for 5 min at 37 °C with PBS containing 10 μM biotin and washed again with cold (4 °C) PBS to remove biotin. After biotin treatment, the cells were fixed with 4% formaldehyde (Polysciences, Inc.) in PBS for 15 min at 20 °C, washed three times in PBS at 20 °C, and made permeable by treatment with 0.1% (v/v) TX100 in PBS for 5 min at 20 °C. The samples were washed with PBS (three times at 20 °C), and nonspecific protein binding sites were blocked by incubation with 3% (w/v) bovine serum albumin (BSA) in PBS (BSA-PBS) for 1 h at 20 °C. The D2R-AP$^{3rd\text{-}loop}$ protein was fluorescently labeled by incubating the cells with a primary mouse monoclonal antibody directed against the extracellular N-terminal FLAG epitope (M2, Sigma-Aldrich; 1:500 dilution in PBS containing 3% (w/v) BSA, 1 h at 20 °C). The cells were washed three times at 20 °C in PBS containing 0.5% (v/v) of the detergent Tween 20. After washing, the cells were incubated (1 h, 20 °C) with BSA-PBS containing Alexa Fluor 594-conjugated goat anti-mouse secondary antibody (Invitrogen; 1:500 dilution) directed against the anti-FLAG mouse monoclonal and Alexa Fluor 488-conjugated streptavidin (Invitrogen; 1:500 dilution) so as to simultaneously label the D2R-AP$^{3rd\text{-}loop}$ protein and the biotinylated D2R-AP$^{3rd\text{-}loop}$, respectively, with fluorescent tags.

The subcellular localization of all the co-expressed biotin ligase fusions, except for Arr-BL, was determined in a separate set of cells by using a primary mouse monoclonal antibody directed against the V5 epitope tag (Invitrogen; 1:1000 dilution) and an Alexa Fluor 488-conjugated goat anti-mouse secondary (Invitrogen; 1:500 dilution). The cells were fixed, made permeable, and stained with the primary and secondary antibodies as described above.

The Arr-BL fusion did not contain a convenient epitope tag. Therefore, to specifically visualize the subcellular localization of arrestin when it was co-expressed with D2R-AP$^{3rd\text{-}loop}$, we utilized an arrestin construct, Arr-YFP, in which arrestin was fused to enhanced YFP. HEK293T cells were co-transfected with cDNA for D2R-AP$^{3rd\text{-}loop}$ substrate and Arr-YFP, fixed using formaldehyde, and then mounted on slides as described above for direct visualization of the fluorescence-enhanced YFP tag by confocal laser microscopy.

All images were obtained using an LSM 5 Pascal laser-scanning confocal microscope (Zeiss), ×63 oil immersion objective. Alexa Fluor 488 and enhanced YFP were excited with the 488-nm line from an argon laser, and Alexa Fluor 594 was excited with the 543-nm line from a helium-neon laser. The signals from the two fluorophores were separated using appropriate emission filters, and the images were created at a resolution of 1024 $\times$ 1024 pixels using a pixel dwell time of 1.6 μs. We ensured that there was no "bleed-through" of signal from one fluorophore into the collection window of the other in the double-labeling experiments by imaging cells labeled with only one of the pair of fluorophores. In these control experiments, no bleed-through was observed even as the laser power was increased 200% over that used to collect the images of the double-labeled samples (*i.e.* cells stained with the anti-FLAG

mouse monoclonal, the Alexa Fluor 594-conjugated goat anti-mouse secondary antibody, and the Alexa Fluor 488-conjugated streptavidin).

Western Blotting and Quantification of Protein Signals—Proteins resolved by SDS-PAGE were transferred to methanol-wetted PVDF membranes by Western blotting using wet electrophoretic elution buffer (25 mM Tris base, 192 mM glycine, 10% (v/v) methanol, 0.1% (w/v) SDS, pH ~8.3). For antibody-based detection, the remaining protein binding sites on the blot were then blocked by incubation with 10% (w/v) nonfat dry milk reconstituted in PBS (1 h at 20 °C). Nonspecific protein binding sites on blots probed with streptavidin for identification of biotinylated proteins were blocked instead by incubating the blot with 3% (w/v) bovine serum albumin in PBS (1 h at 20 °C). V5 epitope-tagged proteins were detected by incubating blots with an HRP-conjugated anti-V5 antibody (Invitrogen; 1:5000 in 10% nonfat milk in 1× PBS). FLAG epitope-tagged protein bands were detected using an HRP-conjugated mouse monoclonal anti-FLAG M2 antibody (Sigma-Aldrich; 1:5000 dilution in 10% nonfat milk in 1× PBS). HA epitope-tagged D2R signal was detected with anti-HA.11 monoclonal antibody (Covance; 1:1000 dilution in 10% nonfat milk in 1× PBS). Biotinylated protein bands were detected using HRP-conjugated streptavidin (Invitrogen; 1:5000 in PBS containing 3% (w/v) BSA). Flotillin was detected with anti-flotillin 1 rabbit polyclonal antibody (Sigma-Aldrich; 1:1000 dilution in 10% nonfat milk in 1×PBS). After incubation with the primary antibodies or HRP-conjugated streptavidin, the blots were washed three times (10 min each) in PBS containing 0.1% (v/v) Tween 20 (PBS-T). If the primary antibody was not directly conjugated to HRP, the membrane was then incubated with appropriate HRP-conjugated secondary antibodies (Jackson Immunoresearch) and washed four times in PBS-T. Chemiluminescent signals catalyzed by the HRP enzyme were obtained using Supersignal West Femto substrate (Pierce-Thermo Fisher Scientific) and detected using a Chemidoc XRS Molecular Imager (Bio-Rad). Images were collected using exposure settings that did not saturate any of the charge-coupled device camera pixels. The intensity of each band was quantified using ImageJ image processing and analysis software (National Institutes of Health, Bethesda, MD). In order to be able to directly compare the signals from the TX100-soluble and -insoluble fractions of a cell sample, the proteins from these fractions were loaded onto the same polyacrylamide gel and transferred to a single blot. The chemiluminescent signals from these fractions were then developed on that blot so that ratio of protein signals from the TX100-soluble and -insoluble fraction accurately represented the ratio of the protein levels in these fractions. Signals from serial dilutions of protein samples were evaluated to ensure that all quantifications were performed in the linear range of the signal protein function.

D2R was visualized as multiple bands on Western blots, and all bands 50 kDa (the approximate molecular mass of the monomeric long form of human D2R) or higher were counted together as the D2R signal from a particular cell sample. Signal that was not specific to D2R expression was identified by examining appropriate control samples, and signal from these non-specific bands was subtracted to estimate the D2R-specific signal.

Relative Biotinylation Efficacy (RBE) Derivations—RBE values were calculated by dividing the percentage of the biotinylated AP fusion that segregated into the TX100-insoluble portion by the percentage of the total parent AP substrate protein that was found there. For example, the percentage of the total biotinylated D2R-AP$^{3rd\text{-}loop}$ that segregated into the TX100-insoluble fraction was ~8%, when biotinylation was mediated by the plasma membrane-targeted biotin ligase NM-BL, although the vast majority (~80%) of the parent D2R-AP$^{3rd\text{-}loop}$ protein substrate is found in that fraction. Consequently, the RBE for the biotinylation of TX100-insoluble D2R-AP$^{3rd\text{-}loop}$ by NM-BL is 8/80, or 0.1, and suggests that biotinylation of D2R-AP$^{3rd\text{-}loop}$ in the TX100-insoluble fraction occurred at only 10% of the frequency of biotinylation of the TX100-soluble D2R-AP$^{3rd\text{-}loop}$ molecules.

Statistical Analyses—Statistical analyses were performed using Microsoft Excel or GraphPad Prism 4 software. The two-sample *t* test for unequal variances with two-tailed *p* values was utilized throughout for comparisons of independent mean values. For multiple comparisons, one way-analysis of variance (ANOVA) was applied and, when applicable, followed by Tukey's post hoc analysis.

RESULTS

The Majority of Plasma Membrane-expressed D2Rs, but Not MORs, Segregate into TX100-insoluble Fractions—Cells transiently expressing either D2R or MOR constructs were treated so as to specifically biotinylate cell surface proteins and then solubilized in a solution of 2% (v/v) TX100 at 4 °C, and the relative levels of biotinylated cell surface receptor segregating into the TX100-soluble and -insoluble cellular fractions were isolated and estimated as described under "Materials and Methods." Greater than 70% of the plasma membrane-expressed wild-type or FLAG-tagged D2R, but less than 30% of MOR, segregated into the TX100-insoluble fraction (Fig. 2, *A–D*).

Dopamine Treatment Reduces the Levels of TX100-insoluble D2R Expressed at the Plasma Membrane—Treatment of the intact cells with dopamine (10 μM for 30 min) decreased the levels of TX100-insoluble plasma membrane-expressed D2R by more than 50% (Fig. 2, *E* and *F*). In contrast, the dopamine-mediated reduction in the levels of cell surface TX100-soluble D2R, was less than 10% (Fig. 2, *E* and *F*) and significantly less than the reduction observed for the TX100-insoluble form.

TX100-insoluble D2R-containing Fractions Do Not Correspond to Canonical Lipid Rafts—Next, we asked if the detergent-insoluble D2R-containing membrane fractions possessed biochemical properties that have been attributed to canonical lipid raft fractions. These biochemical features include 1) resistance to solubilization in cold non-ionic detergents, 2) lower density compared with most other detergent-resistant cell structures, and 3) disruption by cholesterol depletion (6).

HEK293T cell endogenously express flotillin, a conventional marker for lipid raft-containing membrane fractions (27), and we compared the densities of D2R and flotillin-containing TX100-insoluble membrane fractions by layering these mem-

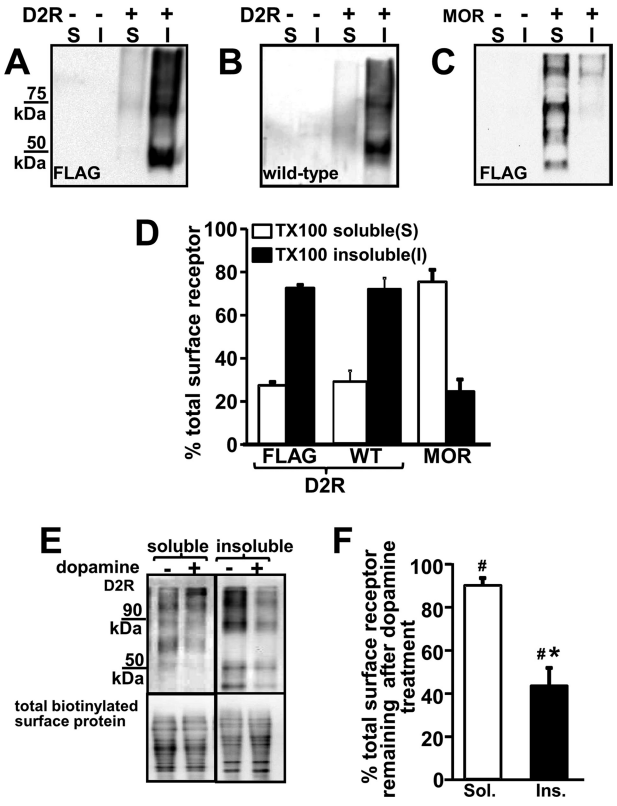

FIGURE 2. **The majority of cell surface (plasma membrane-expressed) D2R segregates into the TX100-insoluble cellular fraction, and dopamine treatment produces a loss of cell surface D2R from both TX100-soluble and -insoluble fractions.** *A*, representative image of a Western blot of cell surface proteins isolated by surface biotinylation from TX100-soluble (*S*) and TX100-insoluble fractions (*I*) from HEK293T cells expressing FLAG-tagged D2R, probed with anti-FLAG antibody. The *left two lanes* are from control cells transfected with empty vector. *B*, representative image of a Western blot, specifically of cell surface proteins, from TX100-soluble (*S*) and TX100-insoluble fractions (*I*) from HEK293T cells expressing wild-type (*WT*) D2R, probed with an antibody targeted against a peptide sequence within the D2R protein. The *left two lanes* are from control cells transfected with empty vector. *C*, representative image of a Western blot, specifically of cell surface proteins from TX100-soluble (*S*) and TX100-insoluble fractions (*I*) from HEK293T cells expressing FLAG-tagged MORs, probed with anti-FLAG antibody. The *left two lanes* are from control cells transfected with empty vector. *D*, quantification of levels of cell surface D2R and MOR constructs that segregate into TX100-soluble (*white bars*) and insoluble (*black bars*) cellular fractions, expressed as a percentage of the total cell surface signal for the respective receptor (mean ± S.E. (*error bars*); $n = 3–4$ separate experiments). *E*, representative image of a Western blot depicting the loss of surface D2R that segregates into TX100-soluble and -insoluble fractions (*top left* and *right panels*, respectively) after dopamine treatment (10 μM, 30 min) of HEK293T cells. The D2R signal was obtained by probing the blots with an antibody directed against the D2R construct. Note that the D2R signals in the blot of TX100-soluble protein (*top left*) cannot be directly compared with the D2R signal in the blot of TX100-insoluble protein (*top right*) because the signal amplification is different across the two *panels*. Western blots, probed with streptavidin, of total biotinylated surface protein segregating into TX100-soluble and -insoluble fractions from the respective cell samples, are depicted in the *bottom panels* and were used as loading controls. However, the effect of dopamine treatment on the levels of D2R segregating into either the TX100-soluble or -insoluble fractions may be discerned. *F*, quantification of D2R remaining in the TX100-soluble (*Sol.*; *white bar*) and insoluble (*Ins.*; *black bar*) plasma membrane fractions after dopamine treatment, expressed as a percentage of surface D2R found in the TX100-soluble or -insoluble fractions, respectively, from cells not treated with dopamine (mean ± S.E.; $n = 5$ separate experiments). Although both TX100-soluble and -insoluble surface D2R fractions were significantly decreased after dopamine treatment (#, $p < 0.05$), the dopamine-mediated decrease in cell surface D2R was significantly greater for the TX100-insoluble fraction (*, $p < 0.01$, *t* test).

branes onto solutions containing increasing concentrations of sucrose. We measured the percentage of each of the proteins that remained buoyant after centrifugation and found that, on average, the D2R-containing TX100-insoluble membrane was significantly denser than membrane containing the lipid raft marker, flotillin (Fig. 3*A*).

Incubation of cells with cholesterol chelating agents, such as MβCD, results in increased detergent solubility of canonical lipid raft proteins (6). As expected, the ratio of TX100-soluble to insoluble flotillin was significantly increased in MβCD-treated HEK293T cells (Fig. 3, *B* and *D*). However, MβCD treatment did not increase the TX100 solubility of D2R (Fig. 3, *B* and *C*).

In-cell Biotin Transfer Assay to Assess Cellular Interactions between D2R and Plasma Membrane-targeted Proteins—The biotinylation interaction assay utilized the *E. coli* biotin ligase, BirA, that specifically biotinylates a unique AP sequence (20). The substrate AP sequence was inserted into D2R, whereas BirA was fused to other cellular proteins, and the D2R-AP substrate and a biotin ligase enzyme fusion were co-expressed in HEK293T cells cultured in biotin-depleted medium. Biotinylation of the AP sequence following a brief treatment of the intact living cells with biotin provides evidence for proximal contact of the D2R-AP substrate and biotin ligase-containing fusion (Fig. 4*A*).

Two D2R-AP fusion constructs were tested: D2R-AP$^{3rd\text{-}loop}$, in which the AP sequence was inserted into the third cytoplasmic loop of FLAG-tagged D2R, and D2R-AP$^{C\text{-}tail}$, where AP was tethered to the D2R C-tail. We found that, as observed earlier with the wild-type and FLAG-tagged D2R construct, the majority of the D2R-AP$^{3rd\text{-}loop}$ (81 ± 2%) and D2R-AP$^{C\text{-}tail}$ (72 ± 2%; mean ± S.E., $n = 6–8$) protein segregated into the TX100-insoluble cellular fraction.

In the first series of experiments, the biotin ligase was targeted to the plasma membrane by fusion with plasma membrane-targeting motifs from either LYN kinase (LYN-BL) (22), KRAS (KRAS-BL) (28), neuromodulin/GAP-43 (NM-BL) (29), or the kinase LCK (LCK-BL) (30).

We then examined the distribution of the D2R-AP substrate that was specifically biotinylated by the above biotin ligase fusions. In contrast to what was observed for the distribution of the parent D2R-AP substrate, in each case, the majority (~86–90%) of the biotinylated D2R-AP was found in the TX100-soluble fraction. Biotinylated D2R-AP was barely detectable in the TX100-insoluble fraction, although most of the D2R-AP substrate is found in this fraction. The results obtained with LYN-BL and KRAS-BL are detailed in Fig. 4, *B–D*, and the inaccessibility of the TX100-insoluble form of D2R-AP to other plasma membrane-targeted biotin ligase fusions is summarized in Fig. 11.

It is important to note that streptavidin, which we used to probe for biotinylated D2R-AP substrates in the Western blots, binds nonspecifically to two bands from HEK293T cells that appear between 50 and 75 kDa. The binding of streptavidin to these bands is nonspecific because it occurs in samples derived from biotin-starved cells and also in the absence of expression of either a biotin ligase or the target AP-containing substrates (see Fig. 4*B*). In addition, we found that the intensity of these

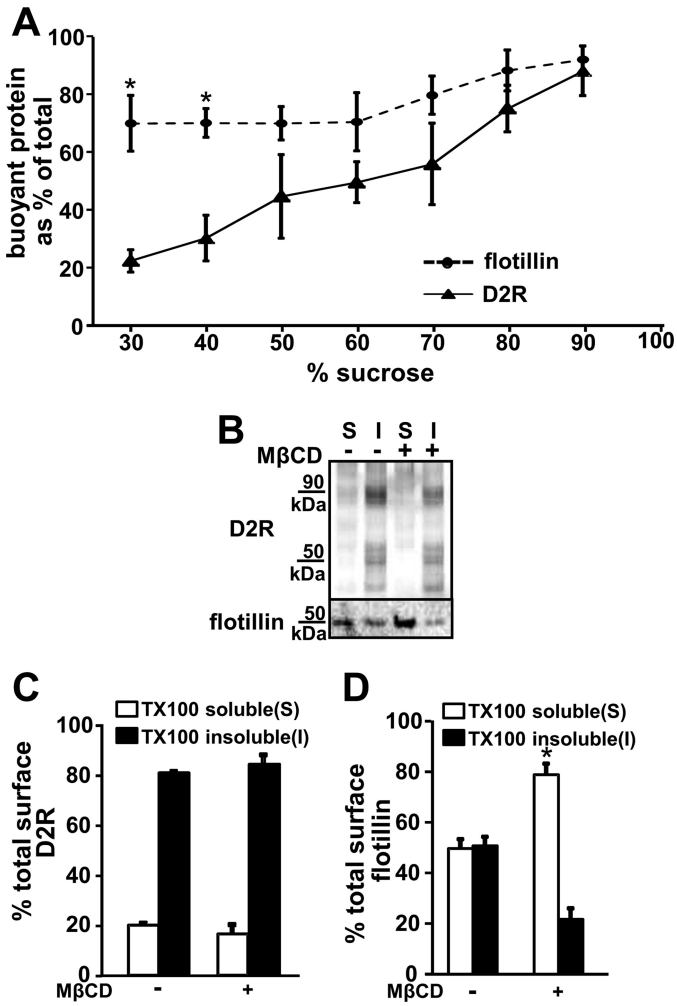

FIGURE 3. **The TX100-insoluble D2R-containing membrane does not correspond to canonically defined lipid raft fractions.** *A*, quantification of the buoyancy of TX100-insoluble D2R or flotillin-containing membrane fractions from HEK293T cells layered onto solutions containing increasing concentrations of sucrose indicates that the D2R-containing TX100-insoluble membrane is on average denser than TX100-insoluble membrane containing flotillin. The graph represents the percentage of the total TX100-insoluble D2R or endogenously expressed flotillin that remained floating at the surface of the indicated sucrose solutions after centrifugation. The *solid line* with *filled triangles* represents the percentage of floating D2R-containing TX100-insoluble membranes. The *dashed line* with *filled black circles* represents the percentage of floating flotillin-containing TX100-insoluble membrane (mean ± S.E. (*error bars*); $n = 4$ separate experiments; *, $p < 0.01$, ANOVA shows significant difference in buoyancy between D2R and flotillin at 30 and 40% sucrose concentrations). *B*, the TX100 solubility of D2R is unaffected by treatment with the cholesterol chelating agent MβCD. Representative image of a Western blot depicting the partitioning into TX100-soluble (*S*) and TX100-insoluble fractions (*I*) of transiently expressed cell surface D2R (*top*) or endogenously expressed flotillin (*bottom*) from HEK293T cells. Samples in *lanes* marked with a *plus sign* were from cell cultures treated with MβCD (10 mM, 1 h, in serum-free medium), whereas samples in *lanes* marked with a *minus sign* were from control cells not treated with MβCD. Cell surface proteins were specifically isolated via cell surface biotinylation. *C*, quantification of the partitioning of cell surface D2R into TX100-soluble (*white bars*) and TX100-insoluble fractions (*black bars*) after MβCD treatment (+) expressed as a percentage of the total cell surface D2R in untreated cells (−) (mean ± S.E.; $n = 3$ separate experiments). *D*, quantification of the partitioning of cell surface flotillin into TX100-soluble (*white bars*) and TX100-insoluble fractions (*black bars*) after MβCD treatment (+) expressed as a percentage of the total cell surface flotillin in untreated cells (−) (mean ± S.E.; $n = 3$ separate experiments; *, $p < 0.05$, significant difference compared with no MβCD treatment, *t* test).

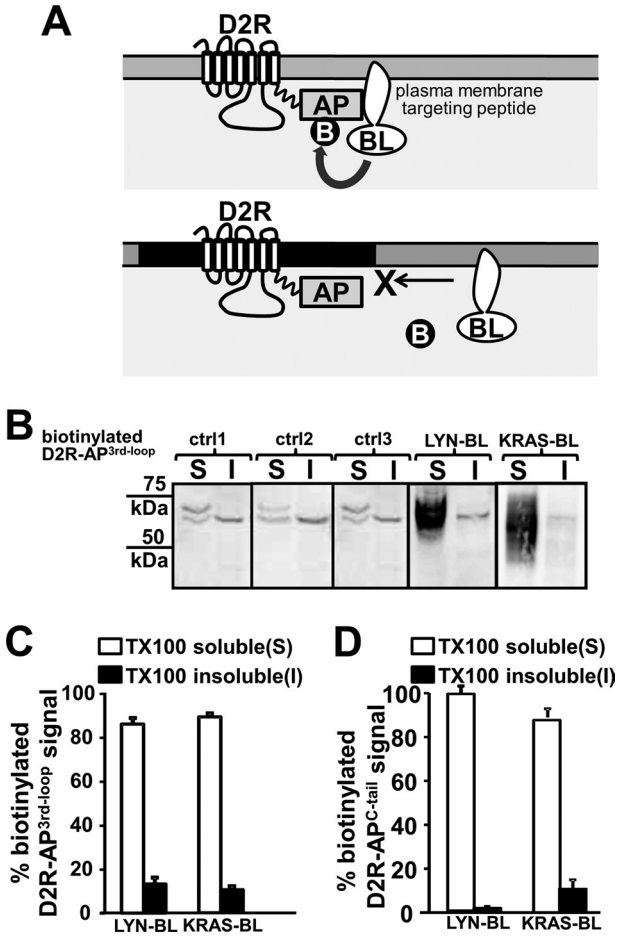

FIGURE 4. **TX100-insoluble D2R-AP fusion substrates exhibit restricted accessibility to multiple plasma membrane-targeted biotin ligases.** *A*, schematic representation of in-cell biotin transfer assay. Proximal interaction of the D2R-AP fusion substrate and BL enzyme-containing constructs allows for the specific attachment of biotin (*B*) to the unique AP sequence. Biotin transfer cannot occur if the biotin ligase enzyme and the AP substrate are unable to interact. *B*, HEK293T cells transiently co-expressing the D2R-AP$^{3rd\text{-}loop}$ construct and either LYN-BL or KRAS-BL were cultured in biotin-depleted medium. The intact cultured cells were then treated with 10 μM biotin for 5 min before solubilization in TX100 solution. The *panel* depicts a representative image of a Western blot of TX100-soluble (*S*) and TX100-insoluble fractions (*I*) derived from the above cell preparations. The blot was probed with HRP-conjugated streptavidin to assess the level of biotinylated D2R-AP$^{3rd\text{-}loop}$ that segregated into either the TX100-soluble or TX100-insoluble biochemical fractions. The *panels labeled LYN-BL* and *KRAS-BL* depict signal from cells transiently co-expressing D2R-AP$^{3rd\text{-}loop}$ and the LYN-BL or KRAS-BL construct, respectively. The *panel labeled ctrl1* (control 1) depicts signal from cells that transiently expressed only D2R-AP$^{3rd\text{-}loop}$ and were not transfected with cDNA for the biotin ligase fusions. The *panel labeled ctrl2* (control 2) depicts signals from cells that transiently expressed only the NM-BL fusion and were not transfected with cDNA for any AP-containing fusion. The *panel labeled ctrl3* (control 3) depicts signal from cells transiently co-expressing D2R-AP$^{3rd\text{-}loop}$ and NM-BL and were not treated with biotin. It is important to note that streptavidin binds nonspecifically to bands that appear between 50 and 75 kDa. The binding of streptavidin to these bands is nonspecific because it occurs in samples derived from biotin-starved cells (*ctrl3*) and in the absence of expression of either biotin ligases (*ctrl1*) or target substrates (*ctrl2*). *C*, quantification of levels of biotinylated D2R-AP$^{3rd\text{-}loop}$ segregated into TX100-soluble (*white bars*) and TX100-insoluble (*black bars*) cellular fractions expressed as a percentage of the total biotinylated D2R-AP$^{3rd\text{-}loop}$ signal (mean ± S.E. (*error bars*); $n = 3$–4 separate experiments). *D*, the experiments described in *B* and *C* were repeated with the D2R-AP$^{C\text{-}tail}$ fusion construct and either LYN-BL or KRAS-BL, respectively, and the graph represents a quantification of the levels of biotinylated D2R-AP$^{C\text{-}tail}$ that subsequently segregated into TX100-soluble (*white bars*) and TX100-insoluble (*black bars*) cellular fractions expressed as a percentage of the total cellular biotinylated D2R-AP$^{C\text{-}tail}$ signal (mean ± S.E.; $n = 3$ separate experiments; ANOVA shows no significant differences in the biotinylation of the TX100-insoluble D2R-AP substrates by the different membrane-targeted ligase constructs, $p = 0.75$).

nonspecific bands relative to the signal from specific biotinylated D2R-AP-containing substrate varies from experiment to experiment (compare Figs. 4*B* and 7*A*). Therefore, in each experiment, control samples from either biotin-starved cells or cells not expressing the biotin ligase or the complementary D2R-AP substrate were used to identify the signal that was specific to biotinylated D2R-AP.

The relative inability of the membrane-targeted biotin ligase enzyme fusion proteins to access and biotinylate D2R-AP substrate that segregated into the TX100-insoluble fraction prompted us to evaluate the TX100 solubility/insolubility of these biotin ligase fusions. The percentage of the plasma membrane-targeted biotin ligase fusions that remained insoluble after treatment with cold TX100 was 83 ± 5% for LYN-BL, 18 ± 6% for KRAS-BL, 50 ± 1% for NM-BL, and 82 ± 3% for LCK-BL (mean ± S.E., $n = 3–5$).

Thus, we have tested the accessibility, in intact cells, of two AP substrate-containing D2R constructs to four different membrane-targeted biotin ligase enzyme constructs that varied widely in their TX100 solubility. In all cases, the D2R-AP substrate molecules that segregated into the TX100-insoluble fraction appeared similarly inaccessible for biotinylation.

Plasma Membrane Localization of Membrane-targeted Biotin Ligase Fusions, LYN-BL and KRAS-BL, and Biotinylated D2R-AP Substrate—To evaluate whether the above biotin ligase enzyme fusion proteins were successfully targeted to the plasma membrane, we utilized confocal laser-scanning light microscopy. The *left* and *right panels*, respectively, in Fig. 5*A* depict the subcellular localization of LYN-BL, a biotin ligase fusion that is predominantly TX100-insoluble, and KRAS-BL, the fusion that segregates predominantly into the TX100-soluble cellular fraction. Both LYN-BL and KRAS-BL were found concentrated at the cell boundaries (Fig. 5*A*), suggesting that these constructs were targeted to the plasma membrane.

Previous studies examining the subcellular localization of D2R in HEK293T, CHO, COS-7, HeLa, NG108-15, and striatal neurons have showed that, although D2R is observed at the plasma membrane, a significant fraction of D2R is retained within intracellular compartments (31–33). We found that the cellular distribution of the D2R-AP$^{3rd\text{-}loop}$ protein was consistent with these previous observations (Fig. 5, *B* and *C*, *left panels*). In contrast, streptavidin staining showed that biotinylation of D2R-AP$^{3rd\text{-}loop}$, which was mediated by LYN-BL or KRAS-BL, occurred predominantly at the cell boundaries and appeared to reflect the plasma membrane targeting of LYN-BL or KRAS-BL (Fig. 5, *B* and *C*, *center panels*).

The Cellular Inaccessibility for Biotinylation Demonstrated by the TX100-insoluble D2R-AP Substrates Does Not Extend to the TX100-insoluble Forms of other AP Substrate-containing Fusion Constructs—We asked if the cellular inaccessibility for biotinylation exhibited by the TX100-insoluble D2R-AP substrates was a common property of all detergent-insoluble membrane-targeted protein molecules. To answer that question, the AP substrate was fused to the plasma membrane-anchoring motif from neuromodulin (NM-AP). The NM-derived plasma membrane-targeting motif has been previously utilized by other investigators to target fusion proteins to detergent-insoluble membrane fractions that have been canonically defined as lipid raft fractions (22, 29). When expressed transiently in HEK293T cells, ~28% of the NM-AP fusion construct segregated into the TX100-insoluble fraction (Fig. 6*A*).

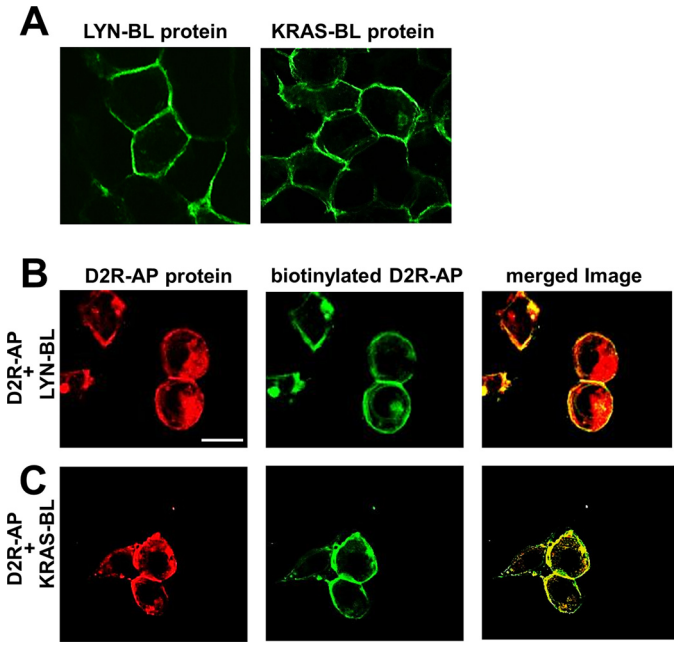

FIGURE 5. **Subcellular localization of LYN-BL, KRAS-BL, D2R-AP$^{3rd\text{-}loop}$, and D2R-AP$^{3rd\text{-}loop}$ that was biotinylated by either LYN-BL or KRAS-BL.** Biotin-depleted HEK293T cells, transiently expressing the indicated protein constructs, were treated with 10 μM biotin for 5 min before staining with the fluorescent dye-conjugated probes. *A*, representative image of the distribution of LYN-BL (*left*) and KRAS-BL (*right*) in cells transiently co-expressing D2R-AP$^{3rd\text{-}loop}$. *B*, *left*, representative image of the distribution of the D2R-AP$^{3rd\text{-}loop}$ protein in cells transiently co-expressing LYN-BL. *Center*, representative image of the distribution of LYN-BL-mediated biotinylation of D2R-AP$^{3rd\text{-}loop}$ visualized by staining with streptavidin conjugated to an Alexa Fluor 488 dye. *Right*, image formed by merging images from the *left* and *center panels*. *Scale bar*, 20 μm. *C*, *left*, representative image of the distribution of the D2R-AP$^{3rd\text{-}loop}$ protein in HEK293T cells transiently co-expressing KRAS-BL. *Center*, representative image of the distribution of KRAS-BL-mediated biotinylation of D2R-AP$^{3rd\text{-}loop}$ visualized by staining with streptavidin. *Right*, image formed by merging images from the *left* and *center panels*.

Biotinylation in intact HEK293T cells of the NM-AP substrate transiently co-expressed with either LYN-BL or KRAS-BL was allowed to occur as described above for the D2R-AP fusions. After the cells were solubilized in cold TX100 solution, we found that the fraction of biotinylated NM-AP that segregated into the TX100-insoluble fraction was comparable and not significantly different from the proportion of the parent NM-AP protein that segregated into that fraction (Fig. 6, *A* and *B*). In other words, the segregation of biotinylated NM-AP into the TX100-soluble and -insoluble fractions paralleled the segregation of the parent NM-AP protein (Fig. 6, *A* and *B*). These results stand in stark contrast to that observed with D2R-AP substrates, where >70% of the parent D2R-AP protein segregates into the TX100-insoluble fraction, but <20% of the biotinylated substrate segregates there. Thus, the inaccessibility to cellular biotinylation exhibited by the TX100-insoluble pool of D2R-AP molecules did not extend to the TX100-insoluble pool of another plasma membrane-targeted AP substrate-containing construct.

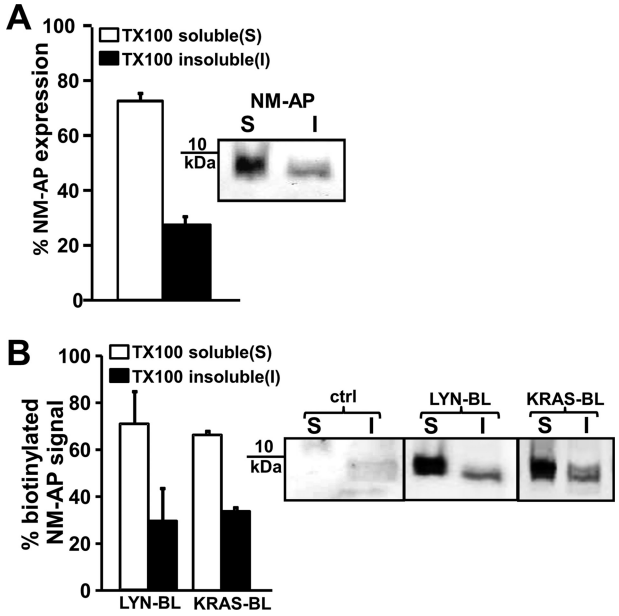

FIGURE 6. **Segregation of the biotinylated NM-AP fusion protein into TX100-soluble and -insoluble cellular fractions after cellular biotinylation mediated by plasma membrane-targeted biotin ligase constructs.** HEK293T cells transiently co-expressing the indicated protein constructs were cultured in biotin-depleted medium. The intact cultured cells were then treated with 10 μM biotin for 5 min before solubilization in TX100 solution. *A*, quantification of the relative levels of NM-AP protein expressed as a percentage of total NM-AP protein signal (mean ± S.E. (*error bars*); $n = 4$ separate experiments). *Inset*, representative image of a Western blot of cells expressing NM-AP and probed with an antibody directed against the NM-AP construct to assess the segregation of the NM-AP protein into these fractions. *B*, quantification of levels biotinylated NM-AP expressed as a percentage of total biotinylated NM-AP (mean ± S.E.; $n = 3$ separate experiments). *Inset*, representative images of Western blots of biotinylated NM-AP substrate by plasma membrane-targeted biotin ligase as indicated. ANOVA indicated no significant differences between the percentage of biotinylated NM-AP substrate recovered in the TX100-insoluble fraction when biotinylation was mediated by the biotin ligases and no significant differences between from the percentage of NM-AP protein and biotinylated NM-AP segregating into the TX100-soluble and insoluble fractions, $p = 0.71$.

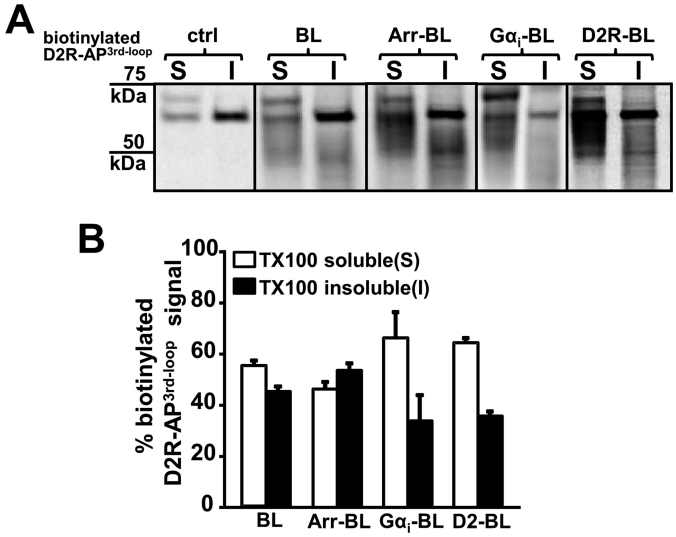

FIGURE 7. **Segregation of biotinylated D2R-AP$^{3rd\text{-}loop}$ fusion constructs into TX100-soluble and -insoluble fractions after cellular biotinylation mediated by various BL fusion constructs.** HEK293T cells transiently co-expressing the indicated protein constructs were cultured in biotin-depleted medium. The intact cultured cells were then treated with 10 μM biotin for 5 min before solubilization in TX100 solution. *A*, representative images of Western blots of biotinylated D2R-AP$^{3rd\text{-}loop}$ after cellular biotinylation mediated by BL, Arr-BL, Gα_i-BL, or D2R-BL. The *leftmost panel* (*ctrl*) depicts a Western blot of membranes from biotin-depleted cells that co-expressed D2R-AP and Arr-BL but were not treated with biotin and allows for distinguishing between the nonspecific signal and the specific signal from the biotinylated D2R-AP substrate. *B*, quantification of levels of biotinylated D2R-AP$^{3rd\text{-}loop}$ expressed as a percentage of total biotinylated D2R-AP$^{3rd\text{-}loop}$ (mean ± S.E., $n = 3$–4 separate experiments; ANOVA indicated no significant differences in the percentage of insoluble D2R-AP$^{3rd\text{-}loop}$ biotinylation by BL, Arr-BL, Gα_i-BL, or D2R-BL, $p = 0.128$).

Cellular Accessibility for Biotinylation of TX100-soluble and -insoluble D2R-AP$^{3rd\text{-}loop}$ and D2R-AP$^{C\text{-}tail}$ Substrates Mediated by 1) V5 Epitope-tagged BL, 2) Gα_i-BL, 3) Arr-BL, and 4) D2R-BL—The *E. coli* biotin ligase, BirA, is a soluble cytoplasmic protein, and hence the BL construct was utilized to test the relative accessibility of the D2R-AP$^{3rd\text{-}loop}$ inserted into the TX100-soluble and -insoluble membrane to freely diffusing cytoplasmic molecules.

It is thought that D2R primarily produces cellular responses via the activation of members of the pertussis toxin-sensitive G_i/G_o family of heterotrimeric G proteins (16, 17). Thus, the Gα_i-BL construct was utilized to evaluate how the two D2R populations interacted with these physiologically important transducers for D2R.

The Arr-BL fusion was constructed to evaluate the relative ability of the D2R populations to interact with arrestins, proteins that serve both as important regulators and mediators of G protein-coupled receptor signals (34). For example, arrestins have been previously shown to interact with D2R to regulate D2R trafficking in an agonist-dependent manner and also serve as mediators of D2R signals (35–37).

Finally, the D2R-BL fusion was constructed to evaluate the accessibility that D2R molecules segregating into the TX100-soluble and -insoluble fractions have for each other.

The biotinylation of the D2R-AP$^{3rd\text{-}loop}$ substrate was initiated in intact HEK293T cells, and the percentage of biotinylated D2R-AP$^{3rd\text{-}loop}$ substrate that subsequently segregated into TX100-soluble and -insoluble cellular fractions is shown in Fig. 7, *A* and *B*. The *control panel* (*ctrl*) in Fig. 7*A* allows for the identification of bands that were not specific to biotinylated D2R-AP substrate.

Confocal Microscopy Examination of the Cellular Localization of BL, Arr-BL, and Gα_i-BL and the Biotinylated D2R-AP$^{3rd\text{-}loop}$ Construct after Coexpression of the Complementary Fusion Proteins—Although BL and Arr-YFP were largely excluded from the nucleus, they were otherwise smoothly and uniformly distributed through the cytoplasm (Fig. 8*A*, *left* and *center panel*, respectively) and their expression pattern was unaffected by the co-expression of D2R constructs.

Previously, we had reported that D2R co-expression alters the subcellular distribution of Gα_{i1} in HEK293T cells (19). In the absence of D2R, the expression of the Gα_{i1} is spread out uniformly through the cytoplasm, and upon D2R co-expression, it moves toward the cell boundaries (19). In accordance with these observations, when co-expressed with D2R-AP$^{3rd\text{-}loop}$, the expression of Gα_i-BL construct was enriched at the cell boundaries (Fig. 8*A*, *right*).

The localization of the D2R-AP substrate that was biotinylated specifically by co-expressed BL, Arr-BL, or Gα_i-BL was

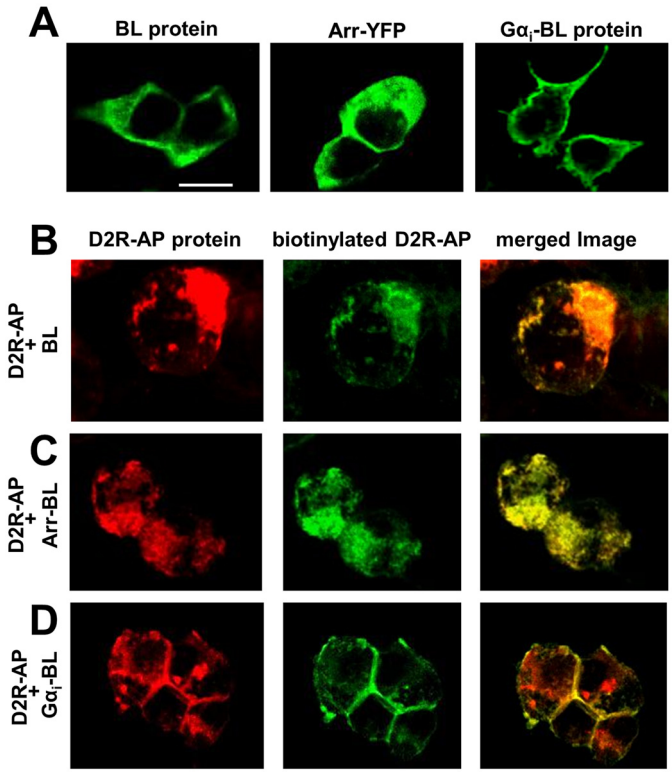

FIGURE 8. **Cellular distribution of BL, Arr-YFP, and Gα$_i$-BL and of D2R-AP$^{3rd\text{-}loop}$ biotinylation mediated by either BL, Arr-YFP, or Gα$_i$-BL.** HEK293T cells transiently expressing the indicated protein constructs were cultured in biotin-depleted medium were treated with 10 μM biotin for 5 min before staining with the fluorescent dye-conjugated probes. *A*, representative image of the distribution of BL (*left*), Arr-YFP (*center*), and Gα$_i$-BL (*right*) in cells transiently co-expressing D2R-AP$^{3rd\text{-}loop}$. *Scale bar*, 20 μm. *B*, *left*, representative image of the distribution of the D2R-AP$^{3rd\text{-}loop}$ protein expressed in cells transiently co-expressing BL. *Center*, representative image of the distribution of D2R-AP$^{3rd\text{-}loop}$ biotinylation mediated by the BL construct and visualized by staining with streptavidin conjugated to the green Alexa Fluor 488 dye. *Right*, image formed by merging images from *left* and *center panels*. *C*, visualization of the biotinylation of D2R-AP$^{3rd\text{-}loop}$ as described in *B*, where the biotinylation was mediated by Arr-BL instead of BL. *D*, visualization of the biotinylation of the D2R-AP$^{3rd\text{-}loop}$ fusion as described in *B*, where the biotinylation was mediated by Gα$_i$-BL instead of BL.

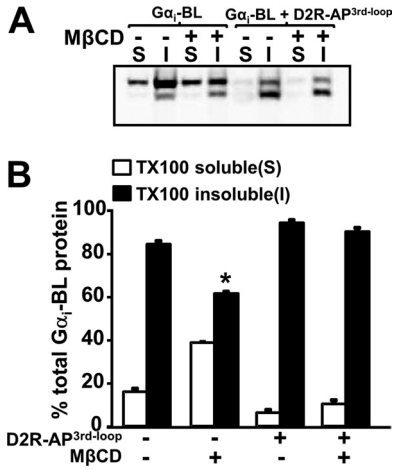

FIGURE 9. **D2R-AP$^{3rd\text{-}loop}$ co-expression abolishes the enhancement of the TX100 solubility of Gα$_i$-BL produced after MβCD treatment.** *A*, representative image of a Western blot of the distribution of transiently expressed Gα$_i$-BL in TX100-soluble and -insoluble cellular. Samples in the *four right lanes* originated from HEK293T cells transiently co-expressing the D2R-AP$^{3rd\text{-}loop}$ construct. *Lanes* labeled with a *plus sign* were from to cell samples treated with MβCD (10 mM, 1 h, in serum-free medium). *B*, quantification of levels of Gα$_i$-BL signal expressed as a percentage of total Gα$_i$-BL (mean ± S.E. (*error bars*); $n = 3$ separate experiments). ANOVA indicated significant differences in the percentage of Gα$_i$-BL distribution within the different treatment groups, $p < 0.0001$. Tukey's post hoc test analysis indicated a significant effect of MβCD treatment on the percentage of Gα$_i$-BL recovered in the insoluble fraction when Gα$_i$-BL was expressed alone, $p < 0.001$, but not when Gα$_i$-BL was expressed with D2R-AP$^{3rd\text{-}loop}$.

visualized by staining with streptavidin. The relative subcellular localization of D2R-AP$^{3rd\text{-}loop}$ protein and the subset of the biotinylated D2R-AP$^{3rd\text{-}loop}$ molecules is illustrated in Fig. 8, *B–D*, respectively. When biotinylation was catalyzed by either BL or Arr-BL, the distribution of biotinylated D2R-AP largely coincided with that of D2R-AP, which was distributed, as illustrated earlier, in an irregular manner throughout the cytoplasm and at the cell boundaries (Fig. 8, *B* and *C*, respectively). When biotinylation was mediated by Gα$_i$-BL, the biotinylated D2R-AP$^{3rd\text{-}loop}$ was found most concentrated at the cell boundaries (Fig. 8*D*). Thus, it may be concluded from the imaging experiments that biotinylation of the D2R-AP substrate occurred in the subcellular regions in which both the D2R-AP and the biotin ligase enzyme fusion were co-expressed (Figs. 5 and 8).

D2R Co-expression Blocks the MβCD-mediated Enhancement of the TX100 Solubility of Gα$_{i1}$—G protein Gα subunits associate with cell membranes via post-translational lipid modifications (38). In addition, it has been shown that a proportion of the cellular Gα$_i$ G protein segregates into detergent-resistant buoyant biochemical fractions that are enriched in cholesterol and sphingolipids (39, 40). We asked if D2R co-expression could alter the "lipid raft properties" of Gα$_i$ subunits, prompted by our previous observation of D2R-mediated relocalization of Gα$_i$ to the plasma membrane.

In accordance with these lipid raft properties, we found that the majority of the Gα$_{i1}$ subunit segregated into the TX100-insoluble fraction and that, in the absence of D2R co-expression, treatment with the cholesterol chelating agent, MβCD (10 mM, 1 h at 37 °C), significantly increased the TX100 solubility of the Gα$_{i1}$ (Fig. 9). Co-expression of D2R significantly decreased the TX100 solubility of Gα$_{i1}$ and prevented the increase in TX100 solubility of Gα$_{i1}$ produced after MβCD treatment (Fig. 9).

Effect of Dopamine Treatment on the Biotinylation of the D2R-AP Substrates—We also examined the effect of dopamine treatment on the biotinylation of both D2R-AP fusion substrates. Cells co-expressing the D2R-AP substrate and a biotin ligase fusion were treated with 10 μM dopamine for 30 min. We examined biotinylation catalyzed by BL, Arr-BL Galphai-BL, and D2R-BL and the plasma membrane-targeted biotin ligase fusions described earlier. A significant dopamine-mediated enhancement of the biotinylation of the D2R-AP substrates was only observed with Arr-BL (Fig. 10).

To visualize the dopamine enhancement of specific biotinylation of the DR-AP substrate, it is important to distinguish between bands produced by nonspecific streptavidin binding and the specific signal produced as a result of biotinylation of the D2R-AP substrate (Fig. 10*A*, compare *top left* and *right panels*).

RBE of TX100-insoluble versus TX100-soluble AP-containing Substrates—To more accurately quantify the relative efficacy at which detergent-insoluble *versus* soluble forms of an AP sub-

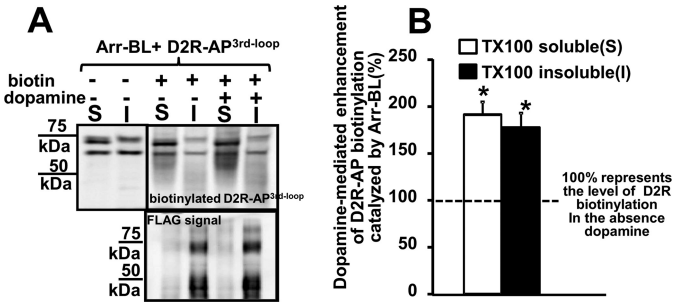

FIGURE 10. **Dopamine-mediated enhancement of D2R-AP$^{3rd\text{-}loop}$ biotinylation mediated by Arr-BL.** HEK293T cells transiently co-expressing the D2R-AP$^{3rd\text{-}loop}$ and Arr-BL were cultured in biotin-depleted medium. The intact cultured cells were then treated with 10 μM biotin for 5 min before solubilization in TX100 solution. *A*, *top*, representative image of a Western blot probed with streptavidin to assess the levels of biotinylated D2R-AP$^{3rd\text{-}loop}$ segregating into TX100-soluble (*S*) and TX100-insoluble (*I*) fractions from HEK293T cells after cellular biotinylation mediated by Arr-BL. *Lanes* labeled with a *plus sign* were from cells treated with dopamine (10 μM, 30 min). The *top left panel* (*ctrl*) depicts a Western blot of membranes from biotin-depleted cells that co-expressed D2R-AP and Arr-BL but were not treated with biotin and allows for distinguishing between the nonspecific signal and the specific signal from the biotinylated D2R-AP substrate. *Bottom*, the levels of D2R-AP$^{3rd\text{-}loop}$ protein in the different cell fractions were assessed by probing the Western blot with an anti-FLAG tag antibody targeted against the D2R-AP$^{3rd\text{-}loop}$ construct and served as the loading control. *B*, quantification of the levels of biotinylated D2R-AP$^{3rd\text{-}loop}$ in TX100-soluble and -insoluble cell fractions after treatment of cells with dopamine expressed as a percentage of the biotinylated D2R-AP$^{3rd\text{-}loop}$ signal from the corresponding cellular fraction (TX100-soluble or -insoluble, respectively) from cells not treated with dopamine (mean ± S.E. (*error bars*); $n = 3$ separate experiments; *, $p < 0.05$, *t* test).

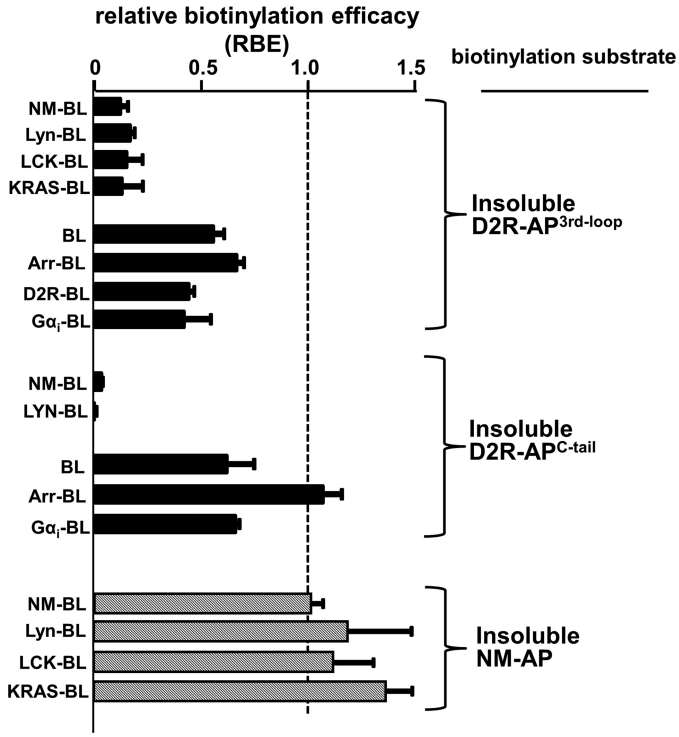

FIGURE 11. **Comparison of the relative biotinylation efficacy of the TX100-insoluble D2R-AP and NM-AP biotinylation substrates obtained with different BirA biotin ligase-containing fusion constructs.** The graph depicts the RBE values (percentage of biotinylated AP substrate segregating into TX100-insoluble fraction/percentage of total AP substrate segregating into the TX100-insoluble fraction) for the biotinylation of the D2R-AP (*black bars*) and NM-AP (*hatched bars*) substrates mediated by the different biotin ligase-containing fusion constructs (mean ± S.E. (*error bars*); $n = 3$–4 separate experiments). ANOVA indicated significant differences between RBEs for the different biotin ligase constructs at D2R-AP$^{3rd\text{-}loop}$ and at D2R-AP$^{C\text{-}tail}$, $p < 0.0001$. Tukey's post hoc analysis indicated no significant differences between RBEs obtained with the different plasma membrane-targeted ligases at either D2R-AP$^{3rd\text{-}loop}$ or D2R-AP$^{C\text{-}tail}$. Tukey's post hoc analysis also indicated no significant differences between RBEs obtained with BL, Arr-BL, Gα_i-BL, or D2R-BL at either D2R-AP$^{3rd\text{-}loop}$ or D2R-AP$^{C\text{-}tail}$. However, RBEs obtained with plasma membrane-targeted biotin ligases at D2R-AP$^{3rd\text{-}loop}$ or D2R-AP$^{C\text{-}tail}$ were significantly less than RBEs obtained with BL, Arr-BL, Gαi-BL, or D2R-BL, $p < 0.05$. Finally, RBEs obtained with NM-AP and the different plasma membrane-targeted biotin ligases were not significantly different from each other. All RBEs obtained with D2R-AP$^{3rd\text{-}loop}$ and at D2R-AP$^{C\text{-}tail}$ with the exception of the D2R-AP$^{C\text{-}tail}$ and the Arr-BL pair were significantly different from 1 (based on 95% confidence intervals). RBEs obtained with NM-AP and the different plasma membrane-targeted biotin ligases were not significantly different from 1 (based on 95% confidence intervals).

strate-containing molecule is biotinylated, it is necessary to account for the unequal segregation of the parent AP substrate into these fractions. To normalize for the unequal distribution of the AP substrates into the TX100-insoluble *versus* the soluble fraction, we divided the percentage of the biotinylated AP fusion, which segregated into the TX100-insoluble portion, by the percentage of the total parent AP substrate protein that was found there. The resulting fraction was termed RBE, which is the efficacy at which the TX100-insoluble AP substrate is biotinylated with respect to the TX100-soluble form. An RBE of less than 1 indicates that a smaller proportion of the AP substrate that segregated into the TX100-insoluble fraction was biotinylated when compared with the TX100-soluble fraction. In other words, AP molecules segregating into the TX100-insoluble fraction were biotinylated at a lower frequency than TX100-soluble molecules and were therefore less accessible for biotinylation. RBE values close to 1 suggest that TX100-insoluble and -soluble molecules are being biotinylated at approximately equal frequencies and were similarly accessible. The RBEs for different pairs of AP substrates and biotin ligase-containing fusion constructs are summarized in the graph depicted in Fig. 11.

DISCUSSION

Several important conclusions may be drawn from an examination of the derived RBE values depicted in Fig. 11.

The Cellular Accessibility, along the Plane of the Plasma Membrane, of the Detergent-resistant Form of D2R Is Severely Limited Relative to the Detergent-soluble Form—RBEs obtained with the D2R-AP substrates and the membrane-targeted biotin ligase fusions, NM-BL, LYN-BL, LCK-BL, and KRAS-BL, were less than 0.2 (Fig. 11), indicating that the biotinylation of the TX100-insoluble D2R-AP substrate molecules by the plasma membrane-targeted biotin ligases occurred at less than 20% of the frequency of the TX100-soluble D2R-AP molecules. Thus, the most plausible explanation is that D2R-AP molecules that segregate into the TX100-insoluble fraction originate from a plasma-membrane structure that exists within living cells to restrict their accessibility to other plasma membrane-associated proteins (*i.e.* they are compartmentalized).

An alternative explanation that could be invoked for the relative inaccessibility of the detergent-insoluble D2R-AP substrates for cellular biotinylation is as follows. D2R adopts two different conformations in living cells: a conformation that is resistant to solubilization and another more detergent-soluble form. By coincidence, the AP substrate was inserted into a region in D2R that is buried in the detergent-insoluble confor-

mation but lies exposed at the surface in the detergent-soluble conformation.

However, the explanation suggested above is unlikely because we tested two different D2R-AP fusions, D2R-AP$^{3rd\text{-}loop}$ and D2R-AP$^{C\text{-}tail}$, with AP insertions at two very dissimilar sites in the D2R molecule. We found that that the TX100-insoluble cellular fractions of both D2R-AP fusions were similarly inaccessible for biotinylation. In fact, in the D2R-AP$^{C\text{-}tail}$ construct, the AP tag was tethered to the end of the D2R C-tail using a long (106-amino acid) flexible linker so as to extend the AP tag away from D2R and allow the AP tag to freely interact with neighboring molecules.

The Detergent-insoluble D2R-containing Microcompartments Probably Contain Gα_i Subunits and Multiple D2R Molecules—It is interesting to note that the RBE values obtained with D2R-AP and Gα_i-BL or D2R-BL fusions were significantly higher than those obtained with D2R-AP and the plasma membrane-targeted biotin ligase fusions (Fig 11). The relatively enhanced accessibility exhibited by Gα_i-BL for the detergent-insoluble fraction of D2R-AP may be explained if Gα_i subunits, as transducers of D2R signals (16, 17), are present together with D2R in the detergent-insoluble microcompartments. One would expect that the frequency of interactions between molecules located within the detergent-resistant D2R compartment is likely to be higher than the frequency of interactions between the compartmentalized D2R and molecules such as LYN-BL that are excluded from the compartment. Further support for such a scenario is provided by the observation that the detergent solubility of Gα_i is not enhanced by treatment with the cholesterol chelating agent, MβCD, after D2R co-expression (Fig. 9) (*i.e.* after D2R co-expression, the Gα_i subunits acquire biochemical properties of the detergent-resistant D2R). The relatively enhanced RBE values obtained with the D2R-AP and D2R-BL (Fig. 11) constructs could be similarly explained if the detergent-insoluble microcompartment structure contained multiple D2R molecules.

The above scenario, with D2R and Gα_i subunits residing together in the detergent-insoluble D2R microcompartments, raises another question. Why was the RBE obtained with Gα_i-BL and the detergent insoluble D2R-AP less than 1 (Fig. 11)? In other words, why did the Gα_i-BL-mediated cellular biotinylation of D2R-AP occur at a lower frequency inside the microcompartment than outside, although it would be reasonable to expect that the D2R-AP substrate molecules and Gα_i-BL enzyme molecules are more closely juxtaposed when they are confined together within microcompartments? This question may be answered if it is postulated that the D2R microcompartment has the properties of a rigid lattice or scaffold within which components, such as the D2R and G protein transducers, are embedded. The lattice could facilitate physiological interactions between the embedded components by orienting the embedded components to contact each other at the physiologically relevant surfaces. Such a rigid lattice could, however, hinder non-physiological interactions occurring between the biotin ligase enzyme and AP substrate inserted artificially into the Gα_i subunits and D2R, respectively. The TX100-soluble D2R-AP, may originate however, from a more fluid portion of the plasma membrane, where both D2R-AP and Gα_i-BL fusions rotate freely to allow the biotin ligase enzyme to better interact with the AP substrate.

Enhanced Accessibility of Cytoplasmic Molecules for Microcompartmentalized D2R—One explanation for the comparatively enhanced RBE exhibited by the soluble biotin ligase constructs, BL and Arr-BL, which can access D2R-AP substrates from the cytoplasm, compared with the plasma membrane-targeted biotin ligase fusions (Fig. 11), is that the compartmentalized detergent-resistant D2R is more accessible from the cytoplasm than from the plane of the membrane.

The In-cell Biotin Transfer Assay with D2R Provides Unambiguous Evidence for the Existence of Plasma Membrane Microcompartments in Living Cells—Alternative explanations from those listed above may be provided for the differing RBEs obtained with the D2R-AP substrates and some of the biotin ligase fusions. However, it is important to note that, with the exception of the D2R-AP$^{C\text{-}tail}$-Arr-BL pair, all of the RBEs obtained for the D2R-AP fusions were significantly less than 1 (Fig. 11). The latter observation unequivocally indicates that the cellular accessibility of the detergent-insoluble D2R is restricted when compared with the detergent-soluble D2R. Because the biotinylation reaction was catalyzed in intact living cells, before the cells were lysed in detergent, it may be concluded that the detergent-resistant D2R molecules are compartmentalized in intact living cells.

Furthermore, the use of the in-cell biotin transfer assay as a valid measure of the relative ability of D2R to interact with other cellular proteins is substantiated by results obtained with Arr-BL. Arrestins are recruited to agonist-bound G protein-coupled receptors, including D2R (35–37), and dopamine treatment significantly enhanced the Arr-BL-mediated biotinylation of both the detergent-soluble and -insoluble forms of D2R-AP fusions. In fact, significant dopamine-mediated enhancement of the biotinylation of the D2R-AP fusions only occurred with Arr-BL (Fig. 10) and not with any of the other BirA biotin ligase-containing fusions.

Both the Detergent-soluble and Microcompartmentalized D2R Forms Respond to Dopamine in Intact Cells and Hence Are Functional—The results with Arr-BL showing dopamine-mediated enhancement of biotinylation of both the detergent-soluble and the compartmentalized detergent-insoluble forms of D2R (Fig. 10) indicate that they represent functional assemblies of the receptor. Furthermore, dopamine treatment results in loss of both detergent-soluble and insoluble forms of D2R from the cell surface (Fig. 2, *E* and *F*). Interestingly, the loss of detergent-insoluble D2R from the cell surface produced by dopamine treatment was significantly greater than that of the detergent-soluble D2R (Fig. 2, *E* and *F*), confirming that the detergent-soluble and -insoluble D2R populations have either intrinsically different biochemistries or originate from distinct biochemical environments in the plasma membrane.

Plasma Membrane Compartmentalization May Be Invoked to Explain Paradoxical Signaling Observations Previously Reported with D2R—Cho *et al.* (36) reported that a D2R-elicited cellular response, thought to be mediated via the second messenger, cAMP, was not desensitized after 40 min of dopamine pretreatment, although such pretreatment caused more than 40% of the receptor to be internalized. It is expected that a

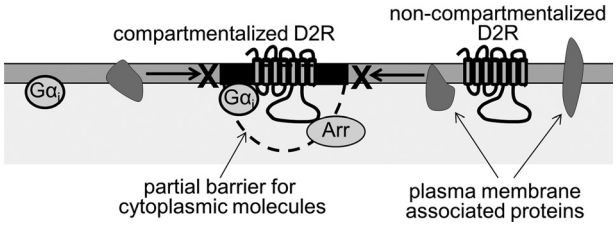

FIGURE 12. **Schematic depicting the two different pools of plasma membrane D2Rs.** D2R is present as expressed in the plasma membrane in either a detergent-resistant (region of the plasma membrane *shaded* in *black*) or detergent-soluble form. The detergent-resistant form is functional and responds to dopamine but is inaccessible to interacting nonspecifically with other plasma membrane proteins and hence is compartmentalized. However, D2R interaction proteins, such as arrestins and G protein $G\alpha_i$ subunits, are able to access the compartmentalized receptor. The detergent-soluble form of D2R originates from a more fluid region of the plasma membrane, allowing the receptor to more readily interact with other plasma membrane proteins.

loss of surface receptor should produce a shift in the dose-response curve to the right, but such a shift was paradoxically not detected. To explain this anomalous result, we hypothesize that the compartmentalized D2R, which we have shown is substantially internalized after dopamine treatment (Fig. 2, *E* and *F*), does not contribute significantly to modulating the cAMP-mediated signal. Instead, the D2R-elicited cellular signal was mediated through the non-compartmentalized D2R, which we show in this report is minimally internalized (Fig. 2, *E* and *F*).

The Detergent-resistant Pool of the Biotinylation Substrate, NM-AP, Which Is Thought to Be Targeted to Hypothetical Lipid Rafts, Does Not Appear to Be Compartmentalized in Living Cells—An important feature of the graph depicted in Fig. 11 is the very different RBEs obtained with D2R-AP and the plasma membrane-targeted NM-AP biotinylation substrates. The RBEs obtained with the NM-AP substrate were not significantly different from 1 (Fig. 11), suggesting that there was no difference between the cellular accessibility of TX100-soluble and -insoluble NM-AP molecules.

The biochemical properties of the plasma membrane-targeting peptide motifs derived from NM, the kinase LCK, and LYN kinase, such as their relatively low detergent solubility, and canonical assumptions about lipid rafts have led to suggestions that they are targeted to lipid raft compartments. Furthermore, these peptide motifs have been used extensively to target other proteins, such as GFP, to these hypothetical structures (22, 29, 30) Similarly, the biochemical properties of the plasma membrane targeting motif from KRAS, such as the relatively high detergent solubility, have been invoked to suggest that it targets to the more fluid detergent-soluble non-raft regions of the plasma membrane (28). However, the RBE values obtained with the NM-AP substrate and NM-BL, LYN-BL, LCK-BL, and KRAS-BL (Fig. 12) were similar and, as stated above, not significantly different from 1. Thus, it may be concluded that 1) the accessibility of the detergent-insoluble form of NM-AP (thought to originate from lipid rafts) to NM-BL, LYN-BL, and LCK-BL (also thought to be predominantly targeted to lipid rafts) is not different from the cellular accessibility to KRAS-BL (which is predicted to be excluded from lipid rafts according to conventional theory); 2) the cellular accessibility of the detergent-soluble form of NM-AP (which is expected to be excluded from lipid rafts according to the lipid raft theory) to NM-BL, LYN-BL, and LCK-BL (lipid raft-targeted) was not different from the accessibility to KRAS-BL (lipid raft excluded); and 3) the accessibility of TX00-insoluble NM-AP (thought to originate from lipid rafts) to all of the above biotin ligase fusions (both raft-targeted and -excluded) was not different from the accessibility of TX100-soluble NM-AP (raft-excluded) to the same set of biotin ligase fusions. In summary, we found that the detergent solubility of NM-AP could not be correlated with compartmentalization of this construct in the plasma membrane, and our application of the in-cell biotin transfer assay was unable to detect any indication of compartmentalization of the presumed lipid raft-targeting peptides in living cells.

The deletion of peptide motifs, like those derived from NM, LYN kinase, and LCK, which are thought to target proteins to lipid rafts, can disrupt the cellular function of the resulting proteins (10). These observations have been cited to argue for the existence of lipid raft compartments in living cells. However, deletion of a protein motif that alters the detergent solubility of the remaining fragment probably produces global alterations in its biochemical properties. Thus, an alternative explanation is that disruption of protein function results not from a failure to be targeted to the hypothetical lipid raft compartment in the cell but rather from a disruption of important intra- and intermolecular interactions.

Thus, we believe that this report of D2R compartmentalization provides the first definitive evidence for plasma membrane microcompartment structure that exists within living cells to restrict the resident molecules from interacting with other plasma membrane and cytoplasmic proteins. Because D2R is a major target of drugs used to treat schizophrenia, depression, and Parkinson disease, our discovery of D2R microcompartmentalization has the potential to alter present assumptions about the mechanism of action of these drugs.

REFERENCES

1. Singer, S. J., and Nicolson, G. L. (1972) The fluid mosaic model of the structure of cell membranes. *Science* **175,** 720–731
2. Lindner, R., and Naim, H. Y. (2009) Domains in biological membranes. *Exp. Cell Res.* **315,** 2871–2878
3. Simons, K., and Sampaio, J. L. (2011) Membrane organization and lipid rafts. *Cold Spring Harb. Perspect. Biol.* **3,** a004697
4. Pike, L. J. (2003) Lipid rafts. Bringing order to chaos. *J. Lipid Res.* **44,** 655–667
5. Simons, K., and Ikonen, E. (1997) Functional rafts in cell membranes. *Nature* **387,** 569–572
6. Simons, K., and Toomre, D. (2000) Lipid rafts and signal transduction. *Nat. Rev. Mol. Cell Biol.* **1,** 31–39
7. Lingwood, D., and Simons, K. (2010) Lipid rafts as a membrane-organizing principle. *Science* **327,** 46–50
8. Lichtenberg, D., Goñi, F. M., and Heerklotz, H. (2005) Detergent-resistant membranes should not be identified with membrane rafts. *Trends Biochem. Sci.* **30,** 430–436
9. Tanner, W., Malinsky, J., and Opekarová, M. (2011) In plant and animal cells, detergent-resistant membranes do not define functional membrane rafts. *Plant Cell* **23,** 1191–1193
10. Brown, D. A. (2006) Lipid rafts, detergent-resistant membranes, and raft targeting signals. *Physiology* **21,** 430–439
11. Shaw, A. S. (2006) Lipid rafts. Now you see them, now you don't. *Nat. Immunol.* **7,** 1139–1142
12. Munro, S. (2003) Lipid rafts. Elusive or illusive? *Cell* **115,** 377–388
13. Heerklotz, H., Szadkowska, H., Anderson, T., and Seelig, J. (2003) The

sensitivity of lipid domains to small perturbations demonstrated by the effect of Triton. *J. Mol. Biol.* **329,** 793–799
14. Heerklotz, H. (2002) Triton promotes domain formation in lipid raft mixtures. *Biophys. J.* **83,** 2693–2701
15. Ritchie, K., Iino, R., Fujiwara, T., Murase, K., and Kusumi, A. (2003) The fence and picket structure of the plasma membrane of live cells as revealed by single molecule techniques (Review). *Mol. Membr Biol.* **20,** 13–18
16. Neve, K. A., Seamans, J. K., and Trantham-Davidson, H. (2004) Dopamine receptor signaling. *J. Recept. Signal Transduct. Res.* **24,** 165–205
17. Missale, C., Nash, S. R., Robinson, S. W., Jaber, M., and Caron, M. G. (1998) Dopamine receptors. From structure to function. *Physiol. Rev.* **78,** 189–225
18. Remington, G. (2003) Understanding antipsychotic "atypicality". A clinical and pharmacological moving target. *J. Psychiatry Neurosci.* **28,** 275–284
19. Celver, J., Sharma, M., and Kovoor, A. (2012) D_2-dopamine receptors target regulator of G protein signaling 9-2 to detergent-resistant membrane fractions. *J. Neurochem.* **120,** 56–69
20. Fernández-Suárez, M., Chen, T. S., and Ting, A. Y. (2008) Protein-protein interaction detection *in vitro* and in cells by proximity biotinylation. *J. Am. Chem. Soc.* **130,** 9251–9253
21. Celver, J. P., Lowe, J., Kovoor, A., Gurevich, V. V., and Chavkin, C. (2001) Threonine 180 is required for G-protein-coupled receptor kinase 3- and β-arrestin 2-mediated desensitization of the μ-opioid receptor in *Xenopus* oocytes. *J. Biol. Chem.* **276,** 4894–4900
22. Zacharias, D. A., Violin, J. D., Newton, A. C., and Tsien, R. Y. (2002) Partitioning of lipid-modified monomeric GFPs into membrane microdomains of live cells. *Science* **296,** 913–916
23. Bünemann, M., Frank, M., and Lohse, M. J. (2003) G_i protein activation in intact cells involves subunit rearrangement rather than dissociation. *Proc. Natl. Acad. Sci. U.S.A.* **100,** 16077–16082
24. Yu, J. Z., and Rasenick, M. M. (2002) Real-time visualization of a fluorescent $G\alpha_s$. Dissociation of the activated G protein from plasma membrane. *Mol. Pharmacol.* **61,** 352–359
25. Shin, B. K., Wang, H., Yim, A. M., Le Naour, F., Brichory, F., Jang, J. H., Zhao, R., Puravs, E., Tra, J., Michael, C. W., Misek, D. E., and Hanash, S. M. (2003) Global profiling of the cell surface proteome of cancer cells uncovers an abundance of proteins with chaperone function. *J. Biol. Chem.* **278,** 7607–7616
26. Ji, Y., Yang, F., Papaleo, F., Wang, H. X., Gao, W. J., Weinberger, D. R., and Lu, B. (2009) Role of dysbindin in dopamine receptor trafficking and cortical GABA function. *Proc. Natl. Acad. Sci. U.S.A.* **106,** 19593–19598
27. Browman, D. T., Hoegg, M. B., and Robbins, S. M. (2007) The SPFH domain-containing proteins. More than lipid raft markers. *Trends Cell Biol.* **17,** 394–402
28. Parton, R. G., and Hancock, J. F. (2004) Lipid rafts and plasma membrane microorganization. Insights from Ras. *Trends Cell Biol.* **14,** 141–147
29. Tong, J., Nguyen, L., Vidal, A., Simon, S. A., Skene, J. H., and McIntosh, T. J. (2008) Role of GAP-43 in sequestering phosphatidylinositol 4,5-bisphosphate to Raft bilayers. *Biophys. J.* **94,** 125–133
30. Krager, K. J., Sarkar, M., Twait, E. C., Lill, N. L., and Koland, J. G. (2012) A novel biotinylated lipid raft reporter for electron microscopic imaging of plasma membrane microdomains. *J. Lipid Res.* **53,** 2214–2225
31. Takeuchi, Y., and Fukunaga, K. (2003) Differential subcellular localization of two dopamine D2 receptor isoforms in transfected NG108-15 cells. *J. Neurochem.* **85,** 1064–1074
32. Prou, D., Gu, W. J., Le Crom, S., Vincent, J. D., Salamero, J., and Vernier, P. (2001) Intracellular retention of the two isoforms of the D_2 dopamine receptor promotes endoplasmic reticulum disruption. *J. Cell Sci.* **114,** 3517–3527
33. Kovoor, A., Seyffarth, P., Ebert, J., Barghshoon, S., Chen, C. K., Schwarz, S., Axelrod, J. D., Cheyette, B. N., Simon, M. I., Lester, H. A., and Schwarz, J. (2005) D_2 dopamine receptors colocalize regulator of G-protein signaling 9-2 (RGS9-2) via the RGS9 DEP domain, and RGS9 knock-out mice develop dyskinesias associated with dopamine pathways. *J. Neurosci.* **25,** 2157–2165
34. Shukla, A. K., Xiao, K., and Lefkowitz, R. J. (2011) Emerging paradigms of β-arrestin-dependent seven transmembrane receptor signaling. *Trends Biochem. Sci.* **36,** 457–469
35. Namkung, Y., Dipace, C., Javitch, J. A., and Sibley, D. R. (2009) G protein-coupled receptor kinase-mediated phosphorylation regulates post-endocytic trafficking of the D2 dopamine receptor. *J. Biol. Chem.* **284,** 15038–15051
36. Cho, D., Zheng, M., Min, C., Ma, L., Kurose, H., Park, J. H., and Kim, K. M. (2010) Agonist-induced endocytosis and receptor phosphorylation mediate resensitization of dopamine D_2 receptors. *Mol. Endocrinol.* **24,** 574–586
37. Allen, J. A., Yost, J. M., Setola, V., Chen, X., Sassano, M. F., Chen, M., Peterson, S., Yadav, P. N., Huang, X. P., Feng, B., Jensen, N. H., Che, X., Bai, X., Frye, S. V., Wetsel, W. C., Caron, M. G., Javitch, J. A., Roth, B. L., and Jin, J. (2011) Discovery of β-arrestin-biased dopamine D2 ligands for probing signal transduction pathways essential for antipsychotic efficacy. *Proc. Natl. Acad. Sci. U.S.A.* **108,** 18488–18493
38. Chen, C. A., and Manning, D. R. (2001) Regulation of G proteins by covalent modification. *Oncogene* **20,** 1643–1652
39. Oh, P., and Schnitzer, J. E. (2001) Segregation of heterotrimeric G proteins in cell surface microdomains. G_q binds caveolin to concentrate in caveolae, whereas G_i and G_s target lipid rafts by default. *Mol. Biol. Cell* **12,** 685–698
40. Patel, H. H., Murray, F., and Insel, P. A. (2008) G-protein-coupled receptor-signaling components in membrane raft and caveolae microdomains. *Handb. Exp. Pharmacol.* **186,** 167–184

Plasma Membrane Compartmentalization of D2 Dopamine Receptors

Meenakshi Sharma, Jeremy Celver, J. Christopher Octeau and Abraham Kovoor

J. Biol. Chem. 2013, 288:12554-12568.
doi: 10.1074/jbc.M112.443945 originally published online March 14, 2013